2018

Isopycnal mixing in the North Atlantic oxygen minimum zone revealed by RAFOS floats

Donald William Rudnickas Jr.
University of Rhode Island, dwrudnickas@gmail.com

ISOPYCNAL MIXING IN THE NORTH ATLANTIC OXYGEN MINIMUM ZONE REVEALED BY RAFOS FLOATS

BY

DONALD W. RUDNICKAS JR.

A THESIS SUBMITTED IN PARTIAL FULFILLMENT OF THE

REQUIREMENTS FOR THE DEGREE OF

MASTER OF SCIENCE

IN

OCEANOGRAPHY

UNIVERSITY OF RHODE ISLAND

2018

MASTER OF SCIENCE THESIS

OF

DONALD W. RUDNICKAS JR.

APPROVED:

Thesis Committee:

Major Professor Jaime B. Palter

H. Thomas Rossby

David L. Hebert

Stephen C. Licht

Nasser H. Zawia

DEAN OF THE GRADUATE SCHOOL

UNIVERSITY OF RHODE ISLAND

2018

ABSTRACT

The Eastern Tropical North Atlantic Oxygen Minimum Zone (OMZ) is a biogeochemically important area in the vicinity of the Cape Verde Islands formed by a combination of biological and physical processes. We use data collected from isopycnal RAFOS floats that were precisely ballasted into two groups and deployed at five locations near the edge of the OMZ. One group was ballasted to drift on the isopycnal where oxygen is at its minimum, and the other group about 300 m deeper. Nearly every six hours for 600 days the floats recorded their positions, temperature, pressure, and (at the isopycnal aligned with the O_2 minimum) dissolved oxygen concentration. Using the record of the float positions at each time interval, we calculate the relative dispersion of pairs of floats. The time derivative of this dispersion provides a diffusivity coefficient that serves to capture the net effect of eddy driven mixing along each isopycnal. With its sluggish mean circulation, the OMZ provided a study area in which this isopycnal mixing is observed with little interference by background advection. The use of Lagrangian subsurface platforms allowed us to investigate the scale dependent nature of two dimensional turbulence. We show that the relative dispersion of the floats in the OMZ area obeyed the canonical 4/3s power scaling that suggests it is representative of two dimensional turbulence. By estimating the de-correlation length scale, we determined that the maximum energy containing eddy length scale in the region is approximately 100 km in the zonal direction and 40 km in the meridional. At this length scale, the effective diffusivity is 1400 ± 500 m^2 s^{-1} in the zonal direction and 800 ± 300 m^2 s^{-1} in the meridional. Within our quantification of error, the diffusivities on the two isopycnals are indistinguishable from one another. We compared the estimate of the diffusivity from the paired dispersion with a tracer-based mixing length method. The magnitude of the diffusivity was similar with the two methods, but

the dispersion method revealed substantial anisotropy that cannot be diagnosed from the mixing length method. We apply the isopycnal mixing coefficient in a simple model aimed at understanding the steady state O_2 budget in the oxygen minimum zone. This model suggests that the vertical structure of the oxygen minimum zone may be set by the vertical profile of biological respiration and that the lateral structure on both isopycnals is set by a balance between the lateral distribution of biological respiration and the zonal and meridional mixing supply of oxygen.

ACKNOWLEDGMENTS

We would like to gratefully acknowledge the support of the National Science Foundation through Award #1736985 and the initial deployment of the sensors through Award #0117660. This project could not have been completed without the hard work of Dr. David Hebert in the deployment phase, his steadfast effort in adapting to the sound source failures, the initial processing of the float data, and in making the data available for analysis.

D. Rudnickas was financially supported in the completion of this degree by the United States Coast Guard and offers his sincerest thanks to Dr. Jonathan Berkson, USCG, for his support and for offering the appointment to the Marine Science Advanced Education Program. D. Rudnickas would also like to express his personal gratitude for the tremendous support and guidance that was provided by the members of the committee: Dr. H. Thomas Rossby, Dr. David Hebert, Dr. Stephen Licht, and especially Dr. Jaime Palter for her unparalleled effort and free expenditure of time, guidance, and friendship.

The altimeter products were produced by Ssalto/Duacs and distributed by Aviso, with support from CNES (http://www.aviso.altimetry.fr/duacs/)

TABLE OF CONTENTS

Page

LIST OF FIGURES

Figure **Page**

LIST OF TABLES

Table **Page**

CHAPTER 1

Introduction

Between the energetic equatorial currents, the anticyclonic subtropical gyre, and the highly productive coastal upwelling zone along the west coast of Africa, lies the Eastern Tropical North Atlantic (ETNA) Oxygen Minimum Zone (OMZ). Here, a combination of biological and physical processes gives rise to a low oxygen tongue in the vicinity of the Cape Verde Islands. Upwelling along the coast and in the OMZ leads to biologically productive surface waters and results in the export of particulate organic carbon through the water column. Remineralization of these particulates below the euphotic zone consumes oxygen. In OMZs, these high rates of respiration occur where the time-averaged circulation is predominantly along streamlines that close about themselves beneath a shallow mixed layer. Therefore, there is no direct advective connection with a well-oxygenated mixed layer, and a low O_2 layer persists beneath the surface (Luyten et al., 1983). The ETNA OMZ oxygen minimum is centered on the $\sigma_\theta = 1027.1$ kg m^{-3} isopycnal at approximately 500 m depth. The core is hypoxic (dissolved oxygen concentrations between 0.4 and 2 ml l^{-1}) and is comprised of a mixture of South Atlantic Central Water and Antarctic Intermediate Water, with a mean water mass age (i.e. time since being at the ocean surface) of over 125 years (Stramma et al., 2016; Gnanadesikan et al., 2013; Brandt et al., 2015).

OMZs are areas of great biogeochemical importance. Low dissolved oxygen concentrations can trigger a shift from aerobic respiration to denitrification which removes bioavailable nitrogen from the oceans, potentially limiting phytoplankton productivity and impacting macrofauna distribution (Deutsch et al., 2011; Deutsch et al., 2015). Reduced productivity diminishes the carbon stored in

the ocean and increases the amount in the atmosphere (Thomas et al., 2004; Codispoti et al., 2001). Stramma et al. (2008) predicted that OMZs would expand with global warming, making the understanding of their formation and maintenance processes of vital importance. The global climate models used for future predictions are known to have major deficiencies in their representation of the intensity of OMZs due to the inability to resolve key processes associated with circulation and mixing (Brandt et al., 2015). Therefore, it is important to develop a better understanding of the balance of processes that form and maintain these regions.

The oxygen budget of a typical OMZ can be broadly defined in terms of a balance between biological oxygen utilization and the net supply of oxygen to the area by advection, lateral mixing, and vertical mixing. Advection by meridionally stacked, eastward flowing zonal jets near the equator and the North Equatorial Countercurrent are thought to be the dominant supply mechanisms of dissolved oxygen to the upper 400 m of the ETNA OMZ, but the velocity of these currents decay with depth and are situated to the south of the ETNA OMZ core so that advection below 400 m at the OMZ core is thought to be weak (Ollitrault et al., 2006; Maximenko et al., 2008; Brandt et al., 2012; Hahn et al., 2014; Brandt et al., 2015; Stramma et al., 2016). There is a permanent cyclonic circulation feature between the Cape Verde Islands and the African coast called the Guinea Dome where isotherms are displaced upward (Siedler et al., 1992; Stramma et al., 2016) and streamlines close about themselves. In this "shadow zone" (Luyten et al., 1983) the dominant supply of oxygen to the core of the OMZ must come from the lateral mixing terms, specifically at and below the O_2 minimum (Gnanadesikan et al., 2013; Hahn et al., 2014; Stramma et al., 2016).

Turbulent mixing is typically parameterized as down-gradient diffusion with a diffusivity coefficient that is a function of the turbulent flow field. Diapycnal mixing results in a down-gradient flux of oxygen to the core mostly from surface waters through the oxycline area of maximum gradient above the OMZ layer and below the mixed layer (Fischer et al., 2013; Brandt et al., 2015) but also from below the OMZ. Recent studies (Fischer et al., 2013; Banyte et al., 2012) have estimated the diapycnal eddy diffusivity through an intentional tracer release and are in good agreement ($\sim 10^{-5}$ m^2 s^{-1}). Eddies also mix tracers along neutral density surfaces, processes often represented as along-isopycnal diffusion, which is thought be the largest supply term of oxygen into the OMZ core (Gnanadesikan et al., 2013; Stramma et al., 2016; Hahn et al., 2014). Estimates of isopycnal diffusivities from baroclinic instability theory (Visbeck et al., 1997) give relatively low values of 100 - 300 m^2 s^{-1}, while a recent tracer release experiment in the ETNA OMZ region gave larger, and highly anisotropic, diffusivities of 500 m^2 s^{-1} in the meridional direction and 1200 m^2 s^{-1} in the zonal direction (Banyte et al., 2013). Meanwhile, uncertainties on the tracer-based diffusivities are 50% of the mean values. Mid-latitude tracer and float experiments have yielded even higher diffusivities (Ledwell et al., 1998). Both intentional tracer studies and theoretical scaling arguments yield estimates of the diffusivities without revealing their time- and space-scale dependence, a problem that can be addressed with Lagrangian floats.

Here, we directly measure isopycnal dispersion by analyzing a set of isopycnal acoustically-tracked RAFOS floats deployed at the edge of the ETNA OMZ. The floats were carefully ballasted and deployed in groups of five to ten at five locations on two isopycnals (Figure 1). The floats recorded their position, pressure, temperature, and (on the isopycnal aligned with the oxygen minimum) dissolved oxygen concentration every six hours for 600 days. These float data provide insight

into the scale-dependent nature of how water is stirred and mixed along constant density surfaces by mesoscale eddies through the calculation of a diffusivity coefficient. The use of RAFOS floats in an area of weak mean circulation such as the ETNA OMZ enables a detailed analysis of Lagrangian methods concurrent with an investigation of OMZ dynamics.

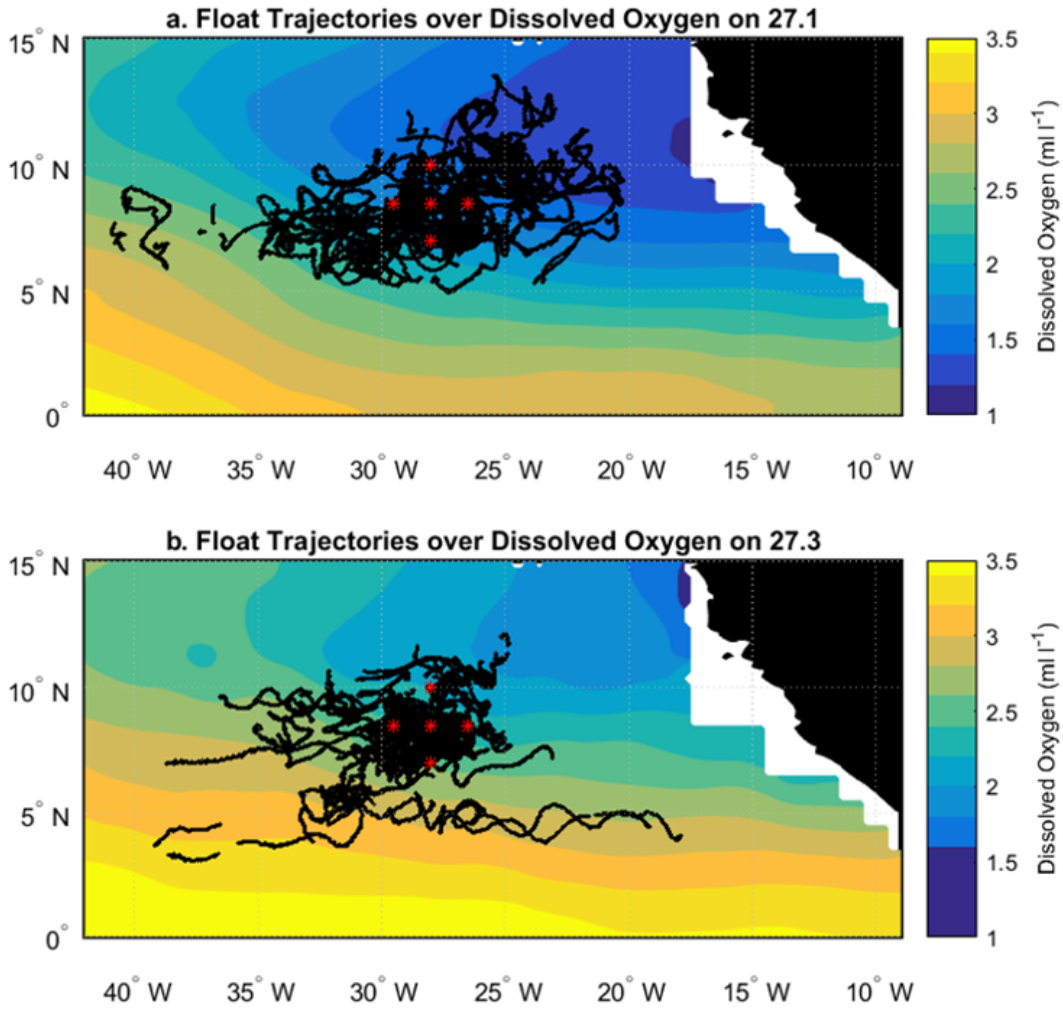

Figure 1: Float trajectories over the WOA13 Dissolved Oxygen Concentration (Garcia et al., 2013) interpolated to the two study isopycnals. The float launch locations are marked by red asterisks.

Following this Introduction, we describe in more detail the data and methods

used to calculate the diffusivity coefficients by two methods: relative dispersion and mixing length (Chapter 2). In Chapter 3, the results of the analysis are presented and compared to similar studies that have used different methods toward the same end. We further discuss the inclusion of chance float pairings into the relative dispersion calculation with their associated benefits and challenges. With a quantification of lateral mixing from the floats, we then apply our results in the simplest model representation of the OMZ to probe the importance of diapycnal and anisotropical isopycnal diffusion in the oxygen budget of the OMZ.

CHAPTER 2

Data and Methods

2.1 Platforms and Sensors

Isopycnal RAFOS floats are Lagrangian platforms that are designed to remain on a surface of constant density and record their position based on the time of reception of an acoustic signal transmitted from a known sound source (Rossby et al., 1986). Ninety-two isopycnal RAFOS floats (50 with Aanderaa oxygen sensors) were purchased from Seascan, Inc. The floats were ballasted to within 0.02 kg m^{-3}. In March and April 2003 the floats and four Webb sound sources were deployed from the R/V SEWARD JOHNSON II near the edge of the ETNA OMZ core (Figure 1). The premature surfacing of a float led to the discovery that the four sound sources had failed after a period ranging from two to five months. Fortunately, French and German sound sources in the area were within range of the floats and provided location information until more sound sources could be deployed. Due to this shift in acoustic coverage from changing sound sources, there was some loss of float position information between mission day 140 and 278. Starting at approximately mission day 278 until 310 there was an almost complete 32-day gap in location information, during which only 3 - 6 floats were receiving acoustic signals (Figure 2).

In total, 82 floats returned data over the 600 day mission. Of these, 45 floats with oxygen sensors were ballasted to follow the σ_θ = 1027.1 kg m^{-3} isopycnal (27.1) at the core of the ETNA OMZ (approximately 400 - 500m) and 37 were for the σ_θ = 1027.3 kg m^{-3} isopycnal (27.3) below the core (700 - 900m). The floats were deployed at five locations near the boundary of the ETNA OMZ (Figure 1) in groups of five to ten floats. With the exception of the transmission gap noted above, the floats recorded their position, time, pressure, and temperature every six

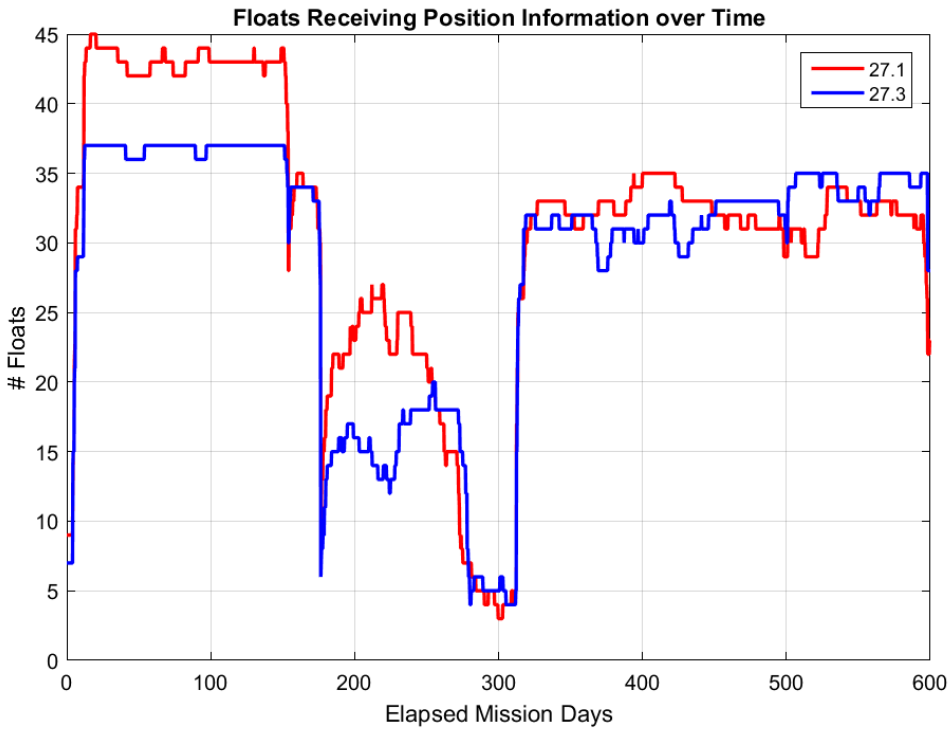

Figure 2: The number of floats on each isopycnal that received information from the sound sources over mission time. Note the decline in number of floats starting at approximately mission day 140 with sharp drops at approximately day 150, 185, and 280. The incorporation of nearby sound sources enabled the recovery of some float position information between day 150 and 310 when new sound sources were deployed.

hours for 600 days. The shallower floats also recorded oxygen concentration.

Figures 3, 4, and 5 compare the temperature and oxygen measurements from the floats against the World Ocean Atlas 2013 climatology (WOA13) (Locarnini et al., 2013; Garcia et al., 2013). Temperature correlated well with the climatology, while the oxygen measured by the floats was systemically lower than the climatology (Figure 5). Figure 4 shows an approximately -0.2 ml l^{-1} oxygen bias from the start as well as a negative drift in the later half of the mission. We suspect this offset to be due to a combination of calibration and drift of the

Aanderaa Oxygen Sensors, as these were early generation instruments known for negative drift over time (D'asaro and McNeil, 2013).

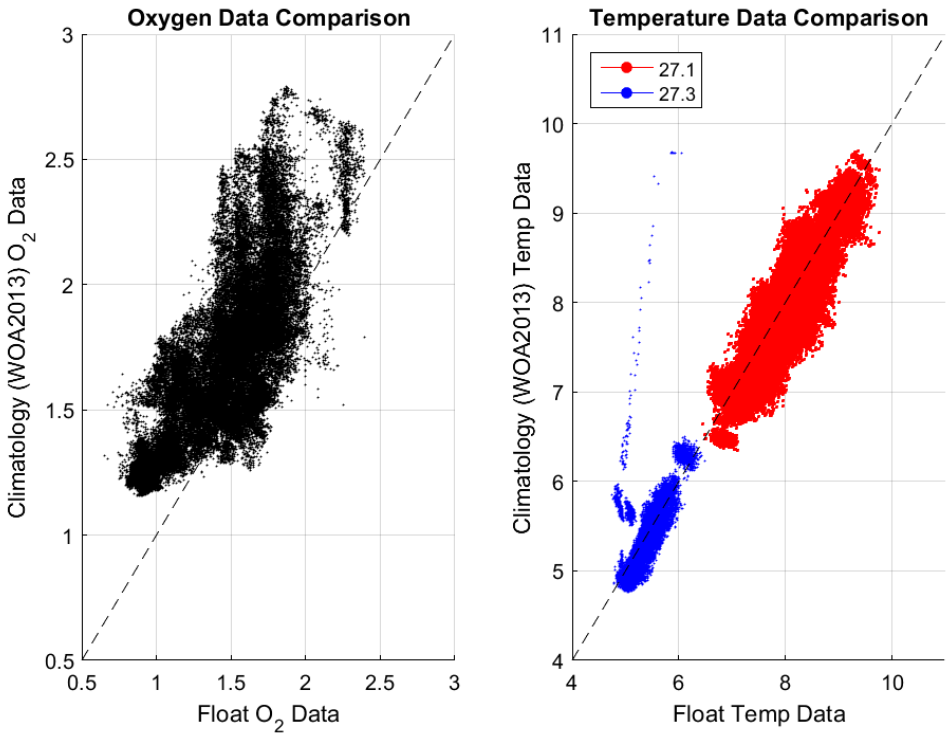

Figure 3: Comparison of the float oxygen (ml l^{-1}; left) and temperature (^{o}C; right) measurements compared to the WOA13 climatology (Garcia et al., 2013; Locarnini et al., 2013).

2.2 Analysis Methods

2.2.1 Relative Dispersion

Relative dispersion of the floats is due to the net effect of turbulence along an isopycnal. Diagnosis of an effective isopycnal diffusivity through relative dispersion was done by tracking float positions over time, as in several previous studies (Klocker et al., 2012; LaCasce, 2008; LaCasce and Bower, 2000; Babiano et al., 1990). Starting with the original float groupings (i.e. those launched at the same time and place), each float's position was compared to the others' at each six-hour time step to measure the separation distance:

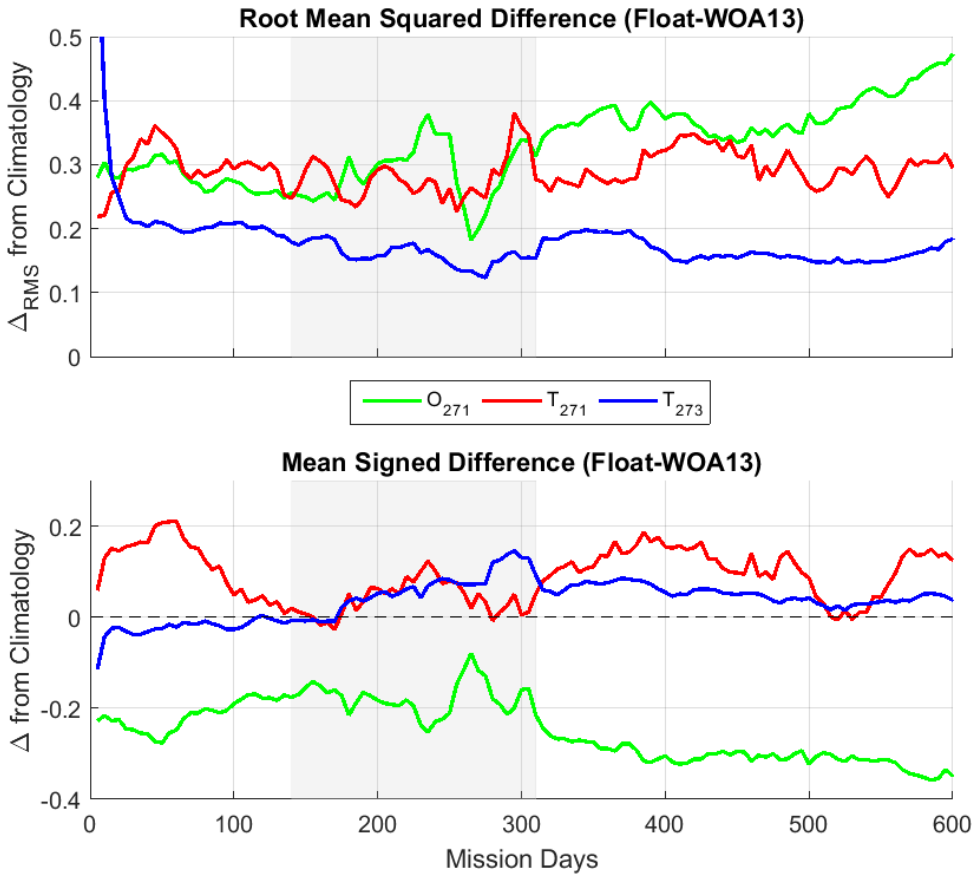

Figure 4: Root mean square (top) and mean signed (bottom) difference of oxygen and temperature from climatology (float - WOA13) over the length of the mission. The time period with sound source issues is shaded in gray. Note the ∼20 day adjustment time at the beginning of the mission especially noticeable with temperature on the 27.3. Also note the approximately linear drift in the oxygen data after recovery from the acoustic failure. We attribute the initial, nearly steady (approx. -0.2 ml l^{-1}) difference in oxygen during the first 400 days to the calibration of the sensors.

$$D(t) = \sqrt{d_x^2(t) + d_y^2(t)} \tag{1}$$

Where $d_x(t)$ and $d_y(t)$ are the zonal and meridional differences in the float pair

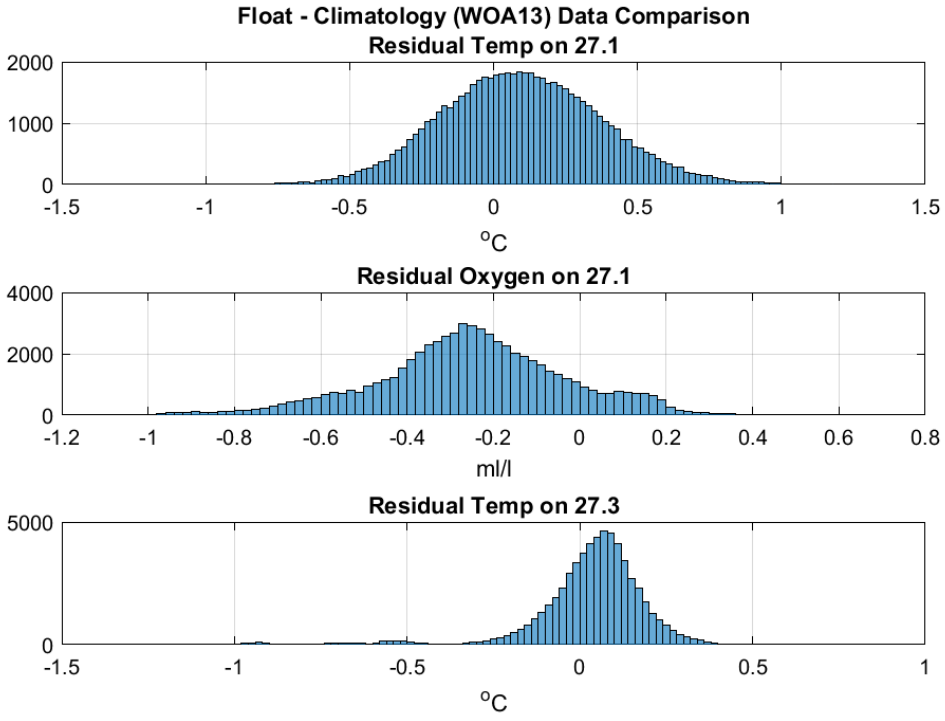

Figure 5: Histogram of float oxygen and temperature measurement residuals. The WOA13 climatology (Garcia et al., 2013; Locarnini et al., 2013) values were subtracted from the float observed values.

positions at the time-step (t). The ensemble mean squared separation distance of all pairs at a given time-step, $\langle D^2 \rangle$, can then be taken as:

$$\langle D^2(t) \rangle = \frac{1}{N} \sum_{pairs} (d_x^2(t) + d_y^2(t)) \tag{2}$$

Where N is the number of float pairings at the time-step, t. The relative diffusivity (K) between two particles is half the time rate of change of the ensemble mean squared separation distance. This, in turn, is twice the absolute diffusivity calculated from a single particle. Since our goal is to calculate the effective diffusivity (Nakamura, 2008) that relates to other parameterizations, we incorporate this second division by two directly into our calculation as in Klocker et al. (2012):

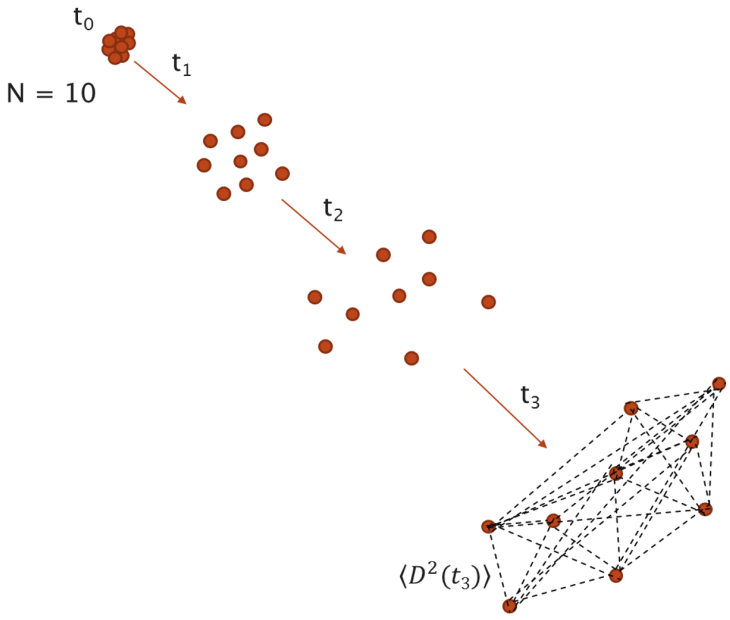

Figure 6: Schematic of the pair dispersion calculation over four time steps with a simulated 10 float group. The dashed lines at t_3 represent the separation distance between the group pairings. $\langle D^2(t)\rangle$ is then the mean of all the squared separation distances at the time step.

$$K = \frac{1}{4}\frac{d}{dt}\langle D^2\rangle \tag{3}$$

The relative diffusivity was quantified in this manner at the oxygen minimum (27.1) and below it (27.3). Next, to quantify the anisotropy in the diffusivity, we repeated the calculation separately for zonal and meridional components of the dispersion in equations 1 and 2 to calculate a K_x and K_y from equation 3.

Because relative dispersion depends on fluctuations at scales comparable with the separation distance between the particle pairs, this method can shed light on physics at different spatial scales (LaCasce and Bower, 2000; LaCasce, 2008; Klocker et al., 2012). By considering the diffusivity in terms of the separation

distance (D), we can make inferences about the size of the eddies in the energy cascade and the dispersion associated with those eddy sizes (Taylor, 1921; Richardson, 1926; Batchelor, 1952; Garrett, 1983; Babiano et al., 1990). The diffusivity is predicted to follow the well-known $D^{4/3}$ law developed by Richardson (1926) where diffusivity increases as the separation distance (D) to the 4/3 power until the floats reach the separation scale of the largest energy containing eddies, at which point individual float velocities become uncorrelated (LaCasce and Bower, 2000).

This $D^{4/3}$ dependence was observed by Richardson in 1926 in his seminal study on the dispersion of smoke plumes from stacks. It was shown mathematically to arise from a scaling argument of turbulent eddy characteristics related to energy cascades. When energy is imparted into a system it is dissipated by smaller and smaller eddies until it reaches the scale of molecular viscosity. In a statistically steady state, the energy imparted at the largest scale will equal the energy dissipated at the smallest scale. The energy dissipation rate, ϵ, with units of $L^2\ T^{-3}$ encapsulates this cascade of energy from large to small scales. Assuming that the characteristic velocity of eddies of various sizes in the cascade depends only on the size of the eddy (d, with units of L) and the dissipation rate (ϵ) (i.e. Kolmogorov (1941)), it follows that the velocity with units of $L\ T^{-1}$ must be:

$$u(d) = A(\epsilon d)^{1/3} \tag{4}$$

with A equal to a dimensionless constant. Diffusivity, with units of $L^2\ T^{-1}$ is a product of a velocity, u (i.e. a perturbation magnitude) and a length scale d (i.e. the range of a perturbation). For a scale dependent diffusivity, we consider the velocity associated with the length scale in the energy cascade (Equation 4) such that the diffusivity must be:

$$K = u(d)\ d = A\epsilon^{1/3}\ \mathbf{d^{4/3}} \tag{5}$$

For distances (d) greater than the maximum length scale allowed by the system, K will asymptote to a constant. We take this constant to be the effective diffusivity of the mesoscale eddies in the region (Richardson, 1926; Kolmogorov, 1941; Taylor, 1921; Lumpkin and Elipot, 2010; Klocker et al., 2012; Cushman-Roisin and Beckers, 2011; LaCasce, 2008).

2.2.2 Chance Pairs

In addition to evaluating Equation 3 using the ensemble of "original pairs" (i.e. those that were intentionally launched at a single time and location), we can also analyze "chance pairs" (i.e. those floats that were either launched at separate locations or separated during the course of their Lagrangian trajectory, and then came within a threshold proximity of one another). The proximity threshold was selected to be 10 km, after being separated by more than that distance for a minimum of five days. 10 km was chosen because it is an order of magnitude less than the size of the mesoscale eddy field that defines the maximum energy containing eddy size in the study area, as further discussed in the Results Section. The five day separation time threshold was selected to be greater than the mean inertial period for the study area (3.5 days) in order to ensure that new pairings were not created every time a pair of floats near the distance threshold completed an inertial oscillation. Our maximum population on the 27.1 (27.3) was 145 (119) original pairs. Using this chance pairing method provided an additional 115 (92) float pairings, nearly doubling the ensemble size at some time steps (Figures A.5, A.6, and A.7). Other threshold values for these parameters were tested, the results of which are shown in Table A.1 and discussed below.

2.2.3 Mixing Length

The floats provide data that can also be used to calculate diffusivity with an independent technique called the mixing length parameterization. The mixing length (L_m) represents the distance a fluid parcel could be transported before significant irreversible mixing occurs. L_m is defined by relating tracer anomalies to the mean gradients on isopycnals (Cole et al., 2015; Armi et al., 1983; Ferrari and Polzin, 2005):

$$L_m = \frac{\langle \sqrt{\overline{Q'Q'}} \rangle}{|\nabla \overline{Q}|} \tag{6}$$

where Q is the tracer (temperature and oxygen used here), $|\nabla \overline{Q}|$ represents the magnitude of the lateral gradient of the mean tracer value in a grid box, which may be provided by the WOA13 climatology or from the bin averaged tracer observations from the floats. The prime indicates perturbation from the mean and the brackets represent an ensemble mean of all float observed perturbations in a grid bin. The study area was divided into geographic bins (0.25^o and 0.5^o were tested) for the purpose of determining the mean and perturbations. The binned means included all float observations over the 600 day mission. Perturbations were determined and separately tested by two methods: first by taking the difference of the observed tracer values at each time step in each geographic bin and the mean tracer value for the bin determined from the float observations. Second, the climatological mean for each bin from the WOA 2013 was subtracted from the float observed value. Given the excellent accuracy of the temperature measurements compared to the climatology discussed above, the calculation of mixing length from temperature was insensitive to this method choice. Because the observed oxygen values were lower than the climatological mean, we only used the oxygen perturbations calculated from the mean of binned observations. The magnitude of

the tracer gradient ($|\nabla\overline{Q}|$) was calculated from the WOA 2013 climatology using a centered difference method for each bin as:

$$|\nabla\overline{Q}| = \sqrt{\left(\frac{d\overline{Q}}{dx}\right)^2 + \left(\frac{d\overline{Q}}{dy}\right)^2} \tag{7}$$

The centered difference gradient was taken from dx and dy set to values ranging from 0.5^o to 6^o and this range of values contributed to the uncertainty. Of note, the mixing length is only taken down the tracer gradient and provides a metric for comparison to the isotropic relative diffusivity calculated above, but provides no means of evaluating anisotropy. The isopycnal diffusivity is proportional to the product of the mixing length and the velocity scale representative of the eddy field:

$$K = c_o L_m U_{rms} \tag{8}$$

where c_o is a mixing efficiency and U_{rms} is the root mean square perturbation velocity calculated from the float trajectories. The mixing efficiency (c_o) was taken as the global average: 0.16 (Wunsch, 1999). The perturbation velocity for each geographic bin was calculated as:

$$U_{rms} = \sqrt{\langle(u_t - \overline{u})^2\rangle + \langle(v_t - \overline{v})^2\rangle} \tag{9}$$

The brackets indicate the ensemble mean of all float velocity perturbations taken as the difference of each float's observed velocity (u_t=$\frac{dx}{dt}$, v_t=$\frac{dy}{dt}$, where x and y are float displacements over a given time interval, t) and the mean float velocity in geographic bins ($\overline{u}$, $\overline{v}$). When calculating the velocities, we tested for sensitivity to various choices: First, we used a "time bin" method to remove the instantaneous effect of inertial oscillations, by calculating the float velocity from displacements over periods (dt) equal to the mean inertial period for the study area (3.5 days or 14

consecutive float records) for both mean and instantaneous velocities. As discussed below, the mixing length was quite sensitive to the duration of the displacements used for calculating float velocity. We also tested the sensitivity of the calculation to a "threshold number;" including only bins that contained a number of float displacements above the a predefined number. The intent was to filter out bins that may have been skewed by only a small number of float measurements but both the mixing length and resultant diffusivity calculations were insensitive to such a mask.

By the mixing length method, diffusivity was calculated using temperature (on both isopycnals) and oxygen (on 27.1) for each geographic bin that included float observations and the mean of these binned values was taken as the effective diffusivity.

2.2.4 Error Calculation

Assuming a normal distribution of pair separation distance at each time step (LaCasce and Bower, 2000), the 90% confidence interval for dispersion was calculated as:

$$\langle D^2(t) \rangle \pm z * \frac{\sigma}{\sqrt{n}} \tag{10}$$

and for diffusivity as:

$$K \pm z * \frac{\frac{1}{2\Delta t}\sqrt{\sigma_t^2 + \sigma_{t+1}^2 - 2\sigma_{t,t+1}}}{\sqrt{n}} \tag{11}$$

where the z score for a normal distribution (1.65 for 90%) was used, σ is the standard deviation of the separation distances at each time step, $\sigma_{t,t+1}$ is the covariance between time steps, and n is the number of pairings at each time step.

In contrast, we estimate the uncertainty on the mixing length calculations, from the range of values resulting from different subjective choices of the terms in Equations 7 and 8. This is discussed in more detail below.

CHAPTER 3

Results and Discussion

Snapshots of the float trajectories over the first 200 days are shown in Figure 7 and the results of our calculation of isopycnal diffusivity from relative dispersion and mixing length methods are provided in detail below.

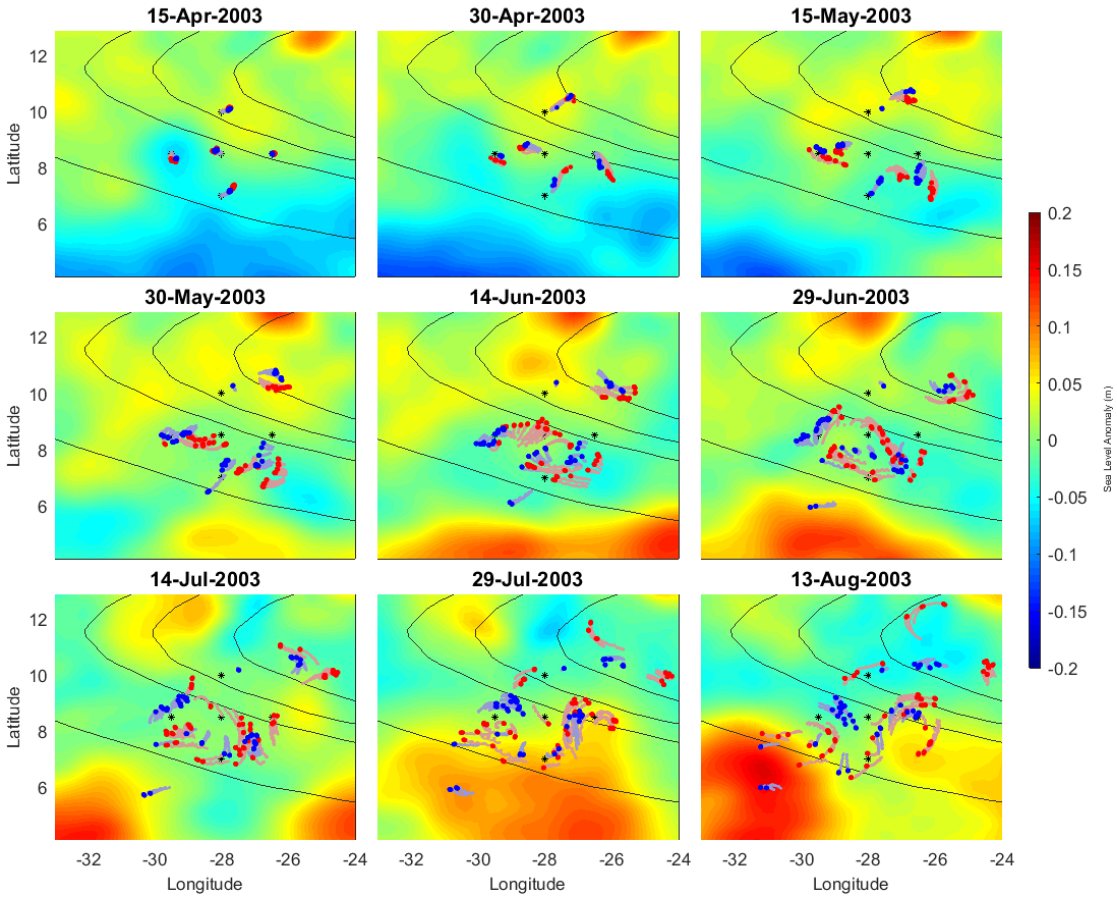

Figure 7: Float positions every 15 days starting on April 15, 2003 for approximately the first 200 days of the mission. The red circles are floats on the 27.1. Blue circles are floats on the 27.3. Gray tails are the previous 14 days' positions. Background color shading is the daily Sea Level Anomaly (m) from AVISO, and the black contours are dissolved oxygen from the WOA 2013 climatology for geographic reference. The black asterisks mark the float launch locations.

3.1 Diffusivity from Relative Dispersion

3.1.1 Anisotropic 2-D Turbulence

Isopycnal diffusivity in the ETNA OMZ was calculated from two-point dispersion of the Lagrangian RAFOS floats as a result of Equation 3 in which the diffusivity, K, is taken as the time derivative of the squared ensemble mean separation distance, $\langle D^2 \rangle$, using a forward difference between consecutive time-steps. At each 0.25 day time-step, the ensemble mean separation distance, $\langle D \rangle$, was calculated as the square root of Equation 2. In order to examine the dependence of K on the length scale, $\langle D \rangle$, the two are plotted against each other in Figure 8. The results are consistent with the dynamics of 2-D turbulence (Richardson, 1926; Babiano et al., 1990; Garrett, 1983), as the diffusivity increases in proportion to the separation distance, $D^{4/3}$ (Figure 8). Further, the dispersion was examined separately in the zonal and meridional directions and was found to be approximately twice as large in the zonal direction as the meridional direction at all length scales (Figure 9).

3.1.2 Largest Energy Containing Eddy Size

The separation length scale at which the motion of a pair of floats become uncorrelated (i.e. the de-correlation scale) is considered an indication of the maximum energy containing eddy size for a system (LaCasce and Bower, 2000; LaCasce, 2008; Klocker et al., 2012). In order to estimate the effective mesoscale diffusivity we assessed the relative diffusivity at this de-correlation length scale. In Figure 8, this length scale can be observed as the point at which there is a shift between the regime where diffusivity increases as $D^{4/3}$ and the high variance region beyond. Visually, Figure 8 suggests that this length scale is approximately 100 - 150 km on both isopycnals. To make a more quantitative estimate, we binned the diffusivity results by separation distance and evaluated the standard deviation

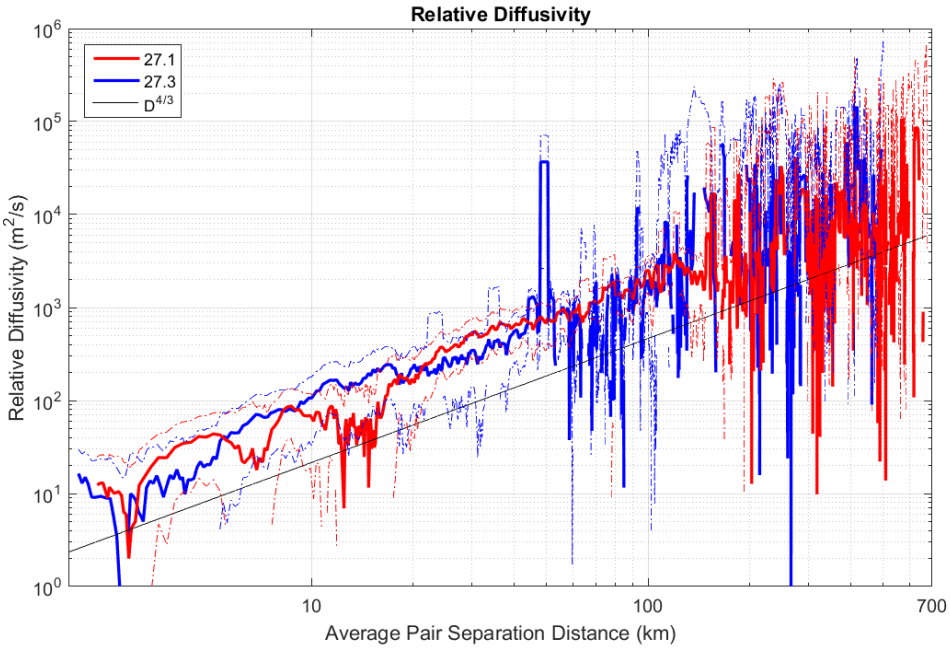

Figure 8: Relative diffusivity calculated from original pairs only shown here smoothed by a 10 km running mean. Note the high noise region on the 27.3 (blue line) at a separation distance between 40 and 100 km; we consider this high variance region to be due to the number of floats still separated by less than 100 km when the sound sources began to fail. The relative diffusivity increases as approximately $D^{4/3}$ until reaching approximately 100 km, the maximum eddy containing eddy size for this area. The dotted lines signify the 90% confidence interval.

from the mean in each bin. The mean was taken by two methods for comparison: a 10 km running mean and in 10 km discrete bins and was only used for visualizing the results and estimating the de-correlation length scale. Figure 10 shows that the standard deviation of the 10 km running mean of the relative diffusivity increases by approximately an order of magnitude at length scales greater than 150 km on the 27.1 isopycnal. Using the standard deviation as a guide, we identified the separation length just prior to the standard deviation consistently increasing from approximately 10^3 to 10^4. We next examined the 90% confidence interval in pair dispersion at that length in the un-binned diffusivity results. Since

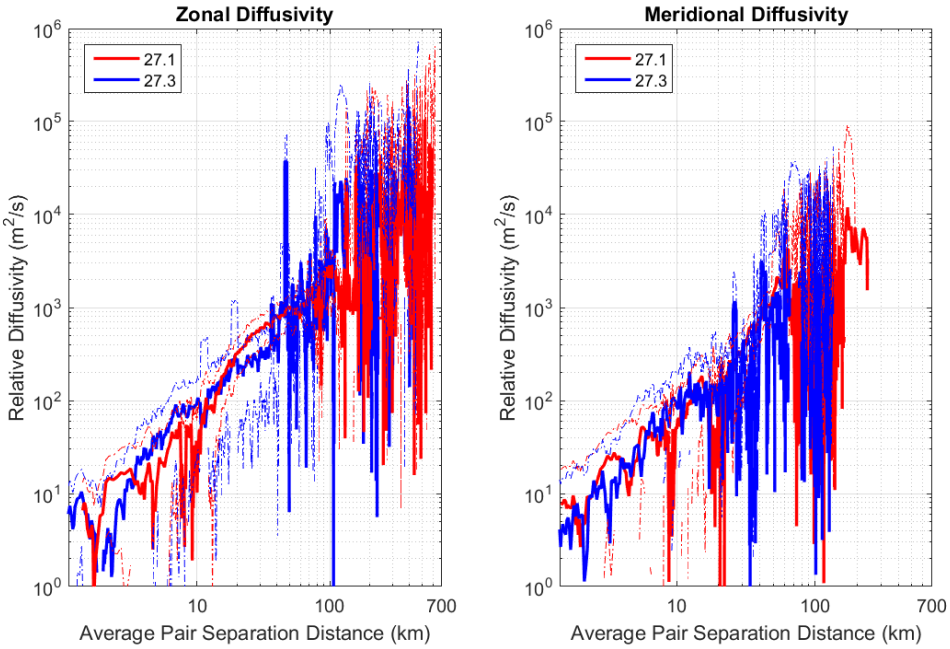

Figure 9: Anisotropy in relative diffusivity calculated from original pairs only. Zonal diffusivity (left) was found to be approximately twice as large as the meridional diffusivity (right). The dotted lines signify the 90% confidence interval.

the confidence intervals are based on the covariance of pair separation distances between time-steps in the calculation of diffusivity (Equation 11), we further refined our approximation of the de-correlation scale by identifying the length where the 90% confidence threshold increased by an order of magnitude or more. The standard deviation and error information helped to narrow the search and the last step of the de-correlation length scale estimation was conducted through analyst interpretation of the un-binned diffusivity results. Here, the diffusivities at each time-step were sorted by mean separation distance at the time-step and examined sequentially from smallest separation distance to largest. The separation distance at which the diffusivity came approximately to a constant was compared to the length at which the error and standard deviation increased and was estimated to be the de-correlation length scale. The approximately constant diffusivity at this

length scale was taken as the effective diffusivity. The results of this evaluation method are shown in Table 1.

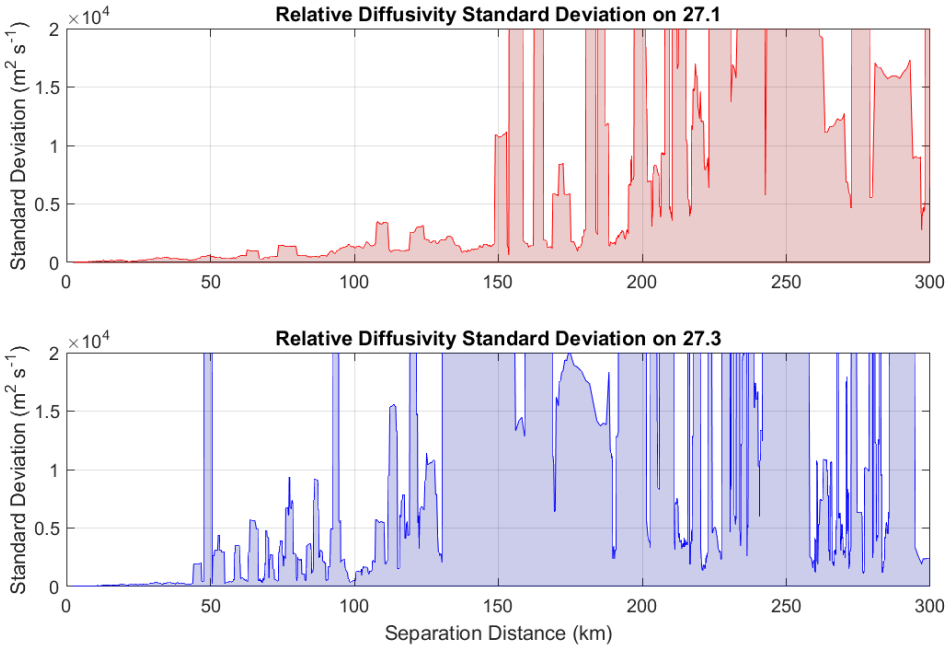

Figure 10: Standard deviation of the original pair relative diffusivity 10 km running mean the on 27.1 (top) and 27.3 (bottom) isopycnals. We use the separation distance at which the standard deviation increases above 10^4 m^2 s^{-1} as the length scale for the maximum energy containing eddies in this region. On the 27.1, this is approximately 150 km and on the 27.3 approximately 115 km. We attribute the spike in standard deviation on the 27.3 isopycnal when floats have a mean separation distance of approximately 50 km to issues with the moored sound sources.

The sound source error presented a challenge to this method. There is an increase in standard deviation on 27.3 at about 40 - 80 km as well as after 100 km. We attribute the increase at the shorter length scale to the acoustic sound source failure beginning around mission day 140. Figure 11 shows the mean separation distance of float pairings on each isopycnal over time. Figure 12 shows the percent of float pairings that are more than 100 km apart. In both figures, the magenta line marks the 140 mission day mark where the sound sources began to fail. While

	Pairs	Effective Diffusivity (m^2 s^{-1}) K	K_x	K_y
Original Only				
27.1	145	**1254**	**1410**	**800**
		± 518	± 493	± 313
Length Scale (km)		90	80	40
27.3	119	**1484**	**1297**	**570**
		± 980	± 630	± 364
Length Scale (km)		100	75	40
Original - 140 day				
27.1	145	**1200**	**1446**	**844**
		± 515	± 597	± 364
Length Scale (km)		91	94	47
27.3	119	**1160**	**1070**	**570**
		± 575	± 806	± 364
Length Scale (km)		101	87	40
Chance Only				
27.1	115	**1198**	**1418**	**357**
		± 1154	± 1000	± 563
Length Scale (km)		100	80	50
27.3	92	**1417**	**1305**	**300**
		± 1271	± 1277	± 250
Length Scale (km)		100	80	40
Chance + Orig				
27.1	296	**1654**	**1747**	**541**
		± 624	± 619	± 376
Length Scale (km)		100	100	70
27.3	211	**1652**	**1479**	**646**
		± 768	± 855	± 884
Length Scale (km)		100	100	70

Table 1: Diffusivity calculated from relative dispersion. These values reflect an effective diffusivity estimated at the the maximum energy containing eddy length scale recorded under each value. The ± row denotes the 90% confidence threshold for each value. The Original-140 day section is the results calculated using only original float pair dispersion over the first 140 mission days in order to exclude any impacts by the acoustic sound source failure. For the chance pair only and chance plus original sections, a 10 km and 5 day threshold for pair identification was used.

∼65% of 27.1 pairings are beyond 100 km at the 140 day mark, only ∼28% of 27.3 pairings are. We therefore interpret the increase in standard deviation on the 27.3 at a mean separation distance less than 100 km as due to the sound source failure.

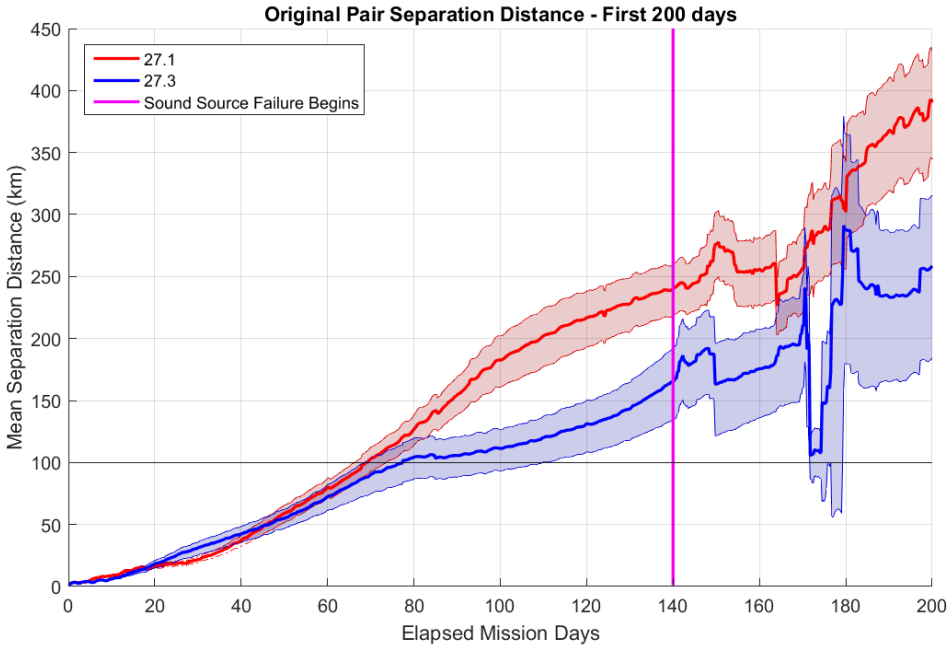

Figure 11: Mean separation distance of original pairs over the first 200 days. The 90% confidence interval is shown in the shading, the magenta line demarks mission day 140 when the sound source failures began, and the black line marks the 100km separation distance. Note that the mean separation distance on both isopycnals is greater than 100km by the time the sound sources begin to fail.

To confirm that 100 km was a good approximation of maximum energy containing eddy length scale on the 27.3 isopycnal given the ambiguity arising from the sound source failure, we conducted the dispersion and diffusivity calculations using only the float positions in the first 140 days, prior to the acoustic failures. Figure 13 and Table 1 show similar diffusivity values to those when all float positions were included but without the variance in the 40 - 80 km range of separation distances, supporting our assertion that the variance in this range in Figure 8 is due to the sound source failures starting at day 140.

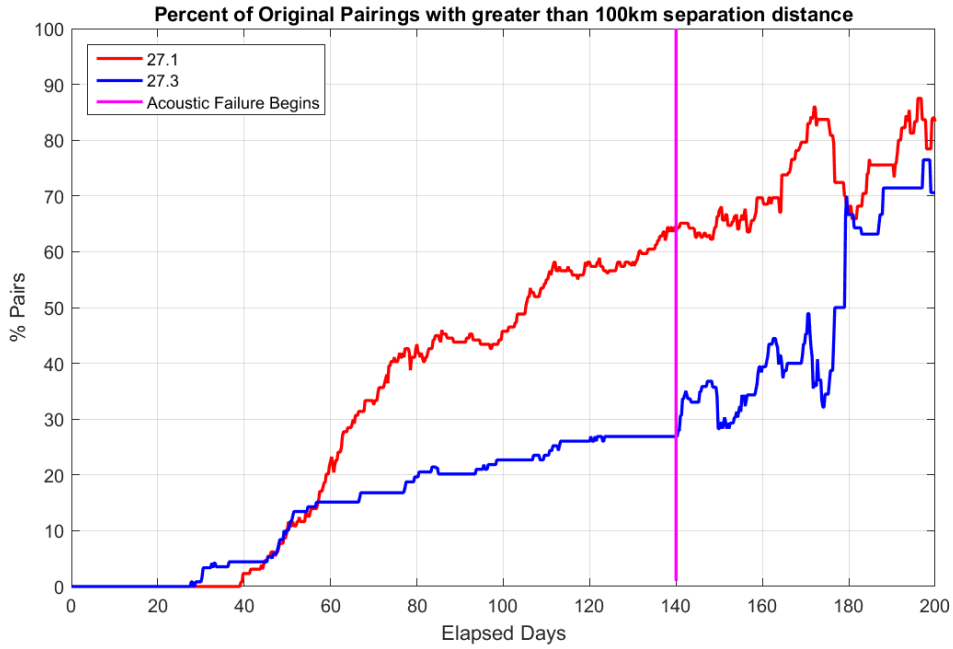

Figure 12: The percent of original pairs with a separation distance of greater than 100km over time. The magenta line demarks mission day 140 when the sound source failures began.

As an additional diagnostic, we looked to the use of chance pairs. Because the elapsed time starts at zero once a pair met a prescribed threshold and is not dependent on the mission day, there is a greater spread in separation distance at the time of the sound source issues. Figure 14 shows the standard deviation in diffusivity compared to separation distance for chance pairs only that came within 10 km of each other after more than five days of separation. This method showed no sign of the earlier increase in standard deviation seen in the original pairings and a similar increase after a separation distance of 100 km.

Our ad-hoc approximation for the size of largest energy containing eddy based on the dispersion statistics corresponds well with the Rossby Radius of Deformation for this area. We calculated the first baroclinic mode radius of deformation from the first baroclinic gravity-wave phase speeds from Chelton et al. (1998). This radius of deformation was between 100 km and 140 km in the study region.

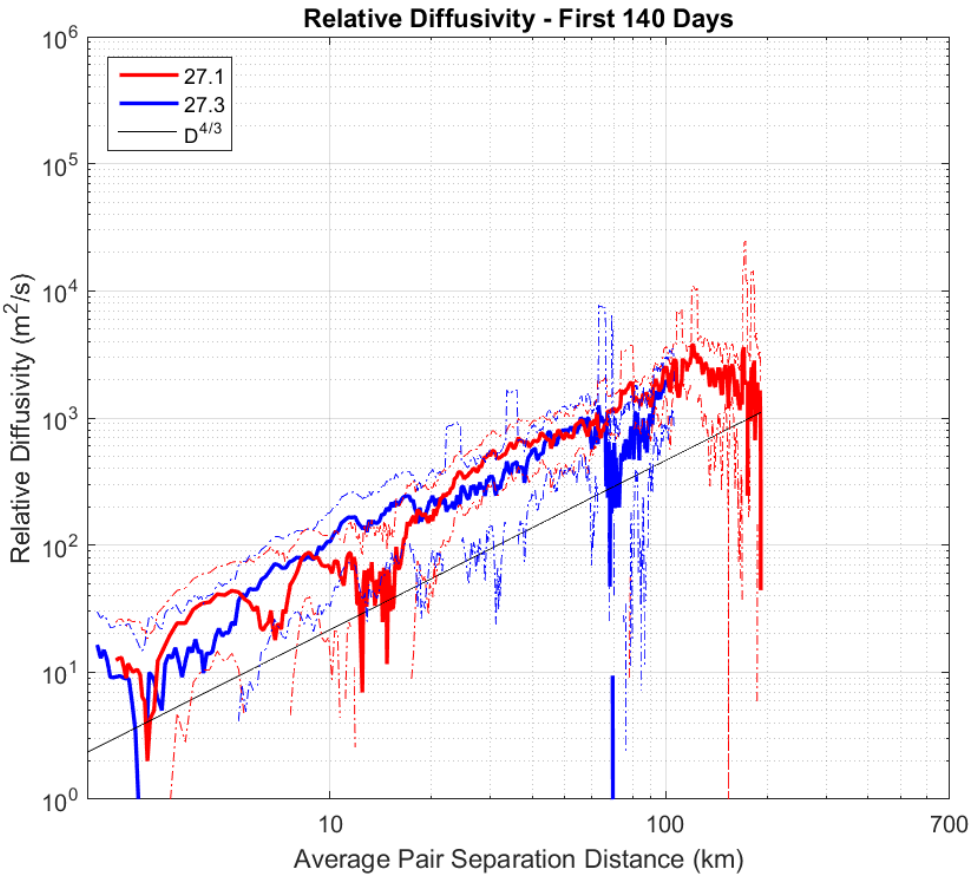

Figure 13: Relative diffusivity calculated only from original pair float dispersion in the first 140 days - prior to the acoustic sound source failures. The results are similar (within the quantification of error) to the results using the entire time-frame but support that the high-variance region from 40-80 km seen in is due to the sound source failures.

Table 1 shows that the approximate de-correlation length scale is roughly the same on both isopycnals and shorter in the meridional direction. Figure 15 shows that on both isopycnals, the floats dispersed in the zonal direction more than the meridional. This anisotropic dispersion agrees with previous work showing that eddies become more ellipsoid closer to the equator with perturbation velocities larger in the zonal than meridional directions (Rypina et al., 2012).

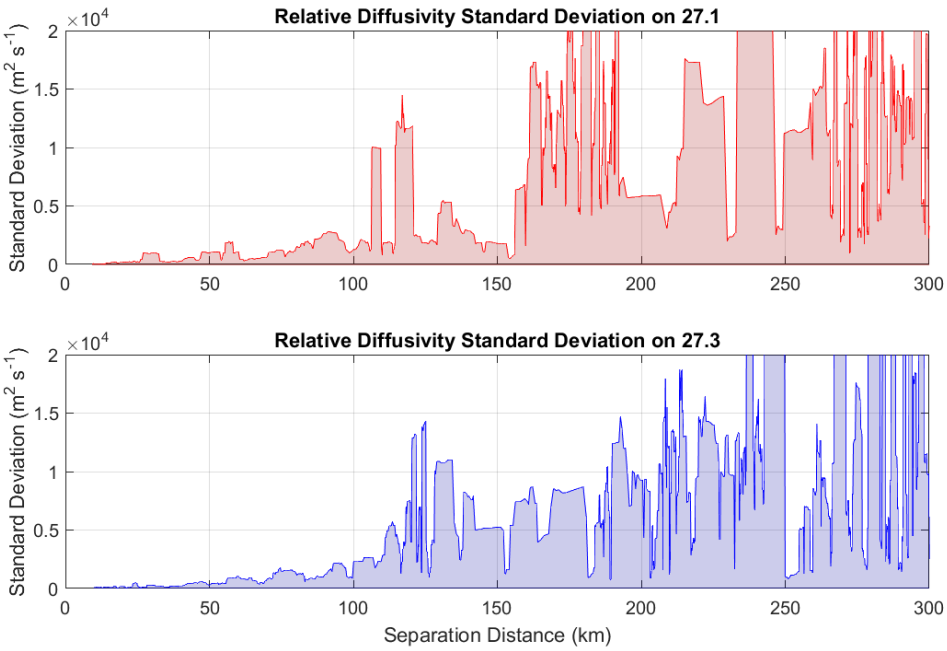

Figure 14: Standard deviation of the chance pairs only (with a threshold of 10km and 5 days) relative diffusivity 10km running mean on 27.1 (top) and 27.3 (bottom). Using chance pairs only, compared to Figure 10, removes the noise that we associate with the sound source failure and shows a length scale for the maximum energy containing eddy on both isopycnals of between 100 - 125 km.

3.1.3 Comparing diffusivity estimates on the two isopycnals

Given the 90% confidence intervals, the diffusivity on the 27.1 and 27.3 isopycnals is virtually indistinguishable (Figure 8). The quantitative similarity is robust whether assessed using original, original plus chance, or chance pairs only. Figure 11 shows the ensemble pair dispersion also nearly identical over the first 80 days at which point the mean pair dispersion exceeds 100 km on both isopycnals.

Isopycnal mixing is known to be the main supply mechanism of oxygen to the OMZ (Gnanadesikan et al., 2013; Fischer et al., 2013; Hahn et al., 2014). Given our result that the turbulent diffusivity is indistinguishable on the two density levels (Figure 8), yet oxygen is much more strongly depleted on the shallower isopycnal

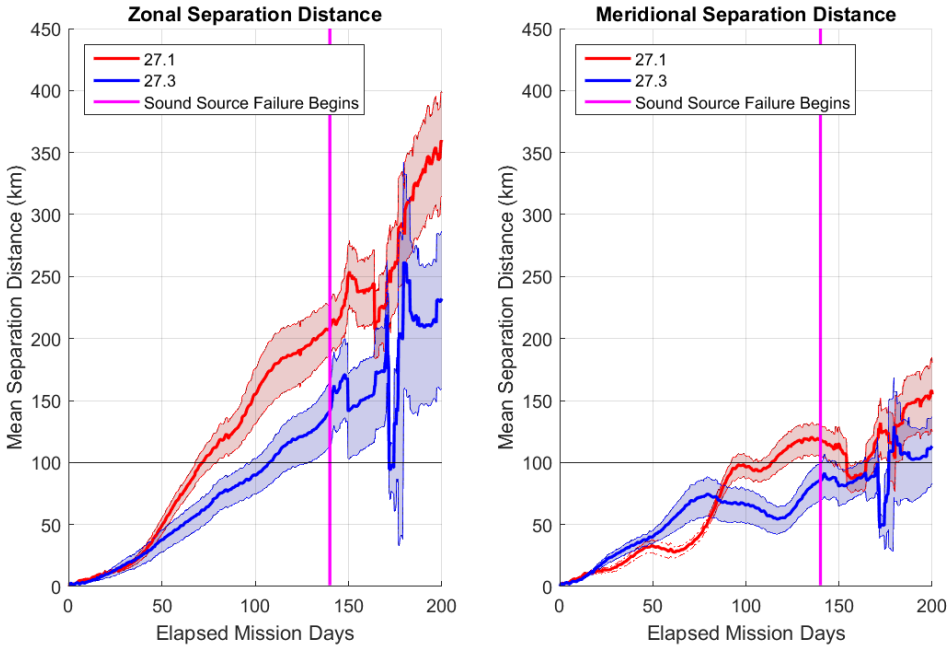

Figure 15: Anisotropy in original pair mean separation distance over the first 200 days. The shaded area signifies the 90% confidence interval.

(Figure 1), we hypothesize that the vertical oxygen gradient arises due to the vertical profile of respiration either locally in the OMZ or in the high productivity narrow coastal upwelling band, that is transported into our study region.

3.1.4 Incorporating Chance Pairs

The benefit of including chance pairings in our analysis was that they helped to fill the time gap generated by the sound source failures given that each chance pairing's elapsed time started at 0 when they met the threshold criteria instead of at launch. Table A.1 summarizes a series of tests conducted with different distance thresholds and shows the number of pairs gained through each threshold choice. The results show nearly identical diffusivity values but with increased error, perhaps because the "chance" encounters may actually be caused by convergent advective features that continue to influence the floats after they are brought

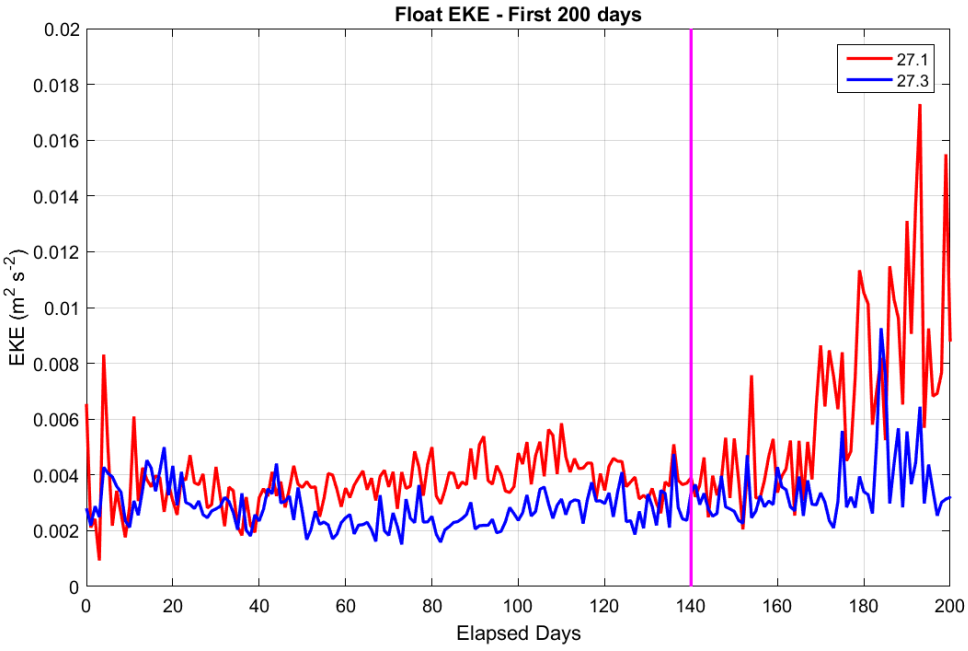

Figure 16: Daily Eddy Kinetic Energy (EKE) calculated from the perturbations of float velocity from the float velocity 0.25^o bin mean for the first 200 days. This is the geographic mean across the study area. The mean EKE on 27.1 was calculated to be 5.3×10^{-3} and 3.5×10^{-3} on 27.3. The magenta line marks mission day 140 when the sound sources began to fail.

together so that not all meetings necessarily describe the processes of dispersion by eddies of increasing size examined here.

3.2 Comparison with other methods and studies

3.2.1 Mixing Length Analysis

Our results for the diffusivity calculated from the mixing length parameterization closely matched the estimates from the float dispersion. Several different sets of values for geographic bin size, time bin size, gradient size, and threshold number were tested. Of these, the mixing length was most sensitive to size of gradient and the diffusivity was most sensitive to the time bin. The range of values resulting from the various parameters were used to estimate the error associated with this method. A subset of the results from the mixing length calculations with a 0.25^o geographic bin are presented in Tables 2 and 3. Overall, we take our mean diffusivity result from mixing length to be 1550 m^2 $s^{-1}\pm$ 600 m^2 s^{-1} on the 27.1 and 1762 m^2 $s^{-1}\pm$ 780 m^2 s^{-1} on the 27.3, which agrees, within the quantification of error, with the isotropic effective diffusivity from relative dispersion. The mixing length on 27.1 is similar to the de-correlation scale determined above and the Rossby Radius of Deformation. The fact that the 27.3 had longer mixing lengths with nearly the same diffusivity makes sense given that the smaller velocities (Figure 16) and smaller gradients (Figure 1) would allow a parcel to travel farther and retain its identifiable characteristics before mixing.

3.2.2 Comparison to results from previous studies

As a comparison to our findings, we summarize here the diffusivities found by several other recent studies using different methods. Recent estimates in the ETNA OMZ region have been smaller than what we diagnosed from float dispersion and the mixing length analysis. A global analysis of lateral diffusivity by mixing length from ARGO floats by Cole et al. (2015), found 500 m^2 s^{-1}(400 m^2 s^{-1}) at 500 m

Mixing Length						
Bin Size	**Threshold #**	**Time Bin**	**Gradient Scale**	**Mean Mixing Length Temp 27.1 (km)**	**Mean Mixing Length Temp 27.3 (km)**	**Mean Mixing Length Oxy 27.1 (km)**
0.25	**0**	14	1	138.77	191.13	116.82
			3	130.15	217.39	118.30
		1	1	120.78	176.59	117.17
			3	114.99	197.55	118.55
	40	14	1	151.05	208.48	149.21
			3	147.21	258.18	150.82
		1	1	144.92	190.71	152.46
			3	143.48	244.40	153.62
			Mean	136.4	210.6	134.6
			STD	**12.3**	**26.4**	**17.0**

Table 2: A subset of mixing length results calculated in 0.25^o geographical bins by Equation 6 using the WOA13 climatology to calculate the means and gradients and float measurements of temperature and oxygen for perturbations. The Threshold # column denotes the minimum number of float records within a bin for the bin to be included in the calculation. The Time Bin column describes the number of 0.25 day increments used to calculate float velocity. A time bin of 1 means that each sequential float position was used to calculate velocity whereas a time bin of 14 means that the velocity was calculated over 14 time-steps. 14 was chosen because it takes the net effect of inertial oscillations with a mean period for this area of 3.5 days instead of the "instantaneous" motions of each oscillation when using 0.25 day increments. The Gradient Scale column identifies the length in degrees over which the tracer gradient was calculated. This was done with a centered difference so that the gradient at each position was taken as the mid point in a line of this scale's length. The mean mixing length columns were taken as the mean value of all 0.25^o bins that contained a quantity of float records exceeding the threshold number and so is a geographic and temporal mean for the study area. The Mean and STD rows take the mean and standard deviation, respectively, of the mixing length results when using the different combinations of parameters.

Diffusivity						
Bin Size	**Threshold #**	**Time Bin**	**Gradient Scale**	**Mean Diffusivity Temp 27.1 (m^2s^{-1})**	**Mean Diffusivity Temp 27.3 (m^2s^{-1})**	**Mean Diffusivity Oxy 27.1 (m^2s^{-1})**
0.25	0	14	1	987	729	698
			3	922	794	707
		1	1	1860	2016	1680
			3	1760	2137	1701
	40	14	1	1278	1290	1188
			3	1254	1522	1199
		1	1	2420	2519	2341
			3	2385	3110	2362
			Mean	1608.1	1764.9	1484.4
			STD	**552.3**	**781.0**	**610.5**

Table 3: Isopycnal diffusivity coefficients calculated in 0.25^o geographical bins by Equation 8 using temperature and oxygen float data. This used the mixing lengths calculated in Table 2, $c_o = 0.16$, and U_{RMS} calculated using the bin-mean float velocities compared to each float's observation for velocity perturbations. The mean diffusivity columns for each tracer were taken as the mean value of all bins that contained a quantity of float records exceeding the threshold number and, as such, is a geographic and temporal mean for the study area. The Mean and STD rows take the mean and standard deviation, respectively, of the mixing length results when using the different combinations of parameters.

(800 m) depth for the ETNA OMZ region. Other mooring and shipboard observations in the area were used to calculate values of 400 (300) $m^2\ s^{-1}$ on 27.1 (27.3) (Brandt et al., 2015) and 750 (250) $m^2\ s^{-1}$ at 500 (800) m (Hahn et al., 2014). An intentional tracer release experiment (Banyte et al., 2013) suggested values closer to the ones we calculated: at 300 m depth $K_y = 500 \pm 200\ m^2\ s^{-1}$ and $K_x = 1200 \pm 600 m^2\ s^{-1}$. Modeling studies of the circulation around the OMZ have typically used smaller diffusivity values than is suggested by our float data: 100 $m^2\ s^{-1}$ (Peña-Izquierdo et al., 2015) to 500 $m^2\ s^{-1}$ (Brandt et al., 2010).

Until now, none of the previous studies have used Lagrangian platforms to address the scale dependent nature of isopycnal mixing. Many also did not account for anisotropy. Our diffusivity results are most similar in magnitude and anisotropy to the results of Banyte et al. (2013), which were measured above the OMZ core.

3.3 Scale Analysis & Model Oxygen Budget Synthesis

To probe the impact of isopycnal mixing on the oxygen budget of the OMZ at the core and below, a scale analysis and simple model was utilized that aimed to explore the oxygen conservation equation on an isopycnal:

$$\frac{dO}{dt} = -JO - u\frac{\partial O}{\partial x} - v\frac{\partial O}{\partial y} + K_x\frac{\partial^2 O}{\partial x^2} + K_y\frac{\partial^2 O}{\partial y^2} + K_z\frac{\partial^2 O}{\partial z^2} \tag{12}$$

Where O is the dissolved oxygen concentration, JO is the dissolved oxygen consumption from biological respiration; u and v are the zonal and meridional velocity components, respectively; K_x and K_y are the zonal and meridional isopycnal eddy diffusivity coefficients, respectively; and K_z is the diapycnal eddy diffusivity coefficient.

The meridional and zonal velocities (u and v) were both set to 0 in order to remove the lateral advection terms from the model equation. This was done to

directly probe the impact of the mixing terms and with full understanding that our model might differ from reality without the small mean advection in the study region. Qualitatively, Figure 1 shows the low mean velocity field given the fact that the floats remained in the study region over the entire 600 day mission. To quantitatively substantiate this assumption, the float displacements over time were geographically binned and averaged to create a quasi-Eulerian mean velocity field (Figures A.1 - A.4). Over the 600 day mission timeframe, the mean velocity was near 0 on both isopycnals in the meridional direction and zonally on the 27.3. The zonal velocity on 27.1, had a mean velocity of -0.1 cm s^{-1}, with a sense of anticyclonic circulation (Figure A.1).

For our scale analysis, we assumed that the system is in steady state and that the time-mean advective supply of oxygen is small, so that Equation 12 reduces to:

$$JO = K_x \frac{\partial^2 O}{\partial x^2} + K_y \frac{\partial^2 O}{\partial y^2} + K_z \frac{\partial^2 O}{\partial z^2} \tag{13}$$

To solve Equation 13, the geographic box of the WOA13 oxygen data interpolated to each isopycnal that contained our float trajectories (4-13^{o}N and 015-045^{o}W) was used to calculate gradients and a point in the center of the box (8.5^{o}N 030^{o}W) was used as a test location. $\frac{\partial^2 O}{\partial x^2}$ was taken along the 8.5^{o}N line of latitude as:

$$\frac{\partial^2 O}{\partial x^2} = \frac{O_{15^oW} - 2O_{30^oW} + O_{45^oW}}{(45^oW - 15^oW)^2} \tag{14}$$

and $\frac{\partial^2 O}{\partial y^2}$ along the 030^{o}W line of longitude as:

$$\frac{\partial^2 O}{\partial y^2} = \frac{O_{13^oN} - 2O_{8.5^oN} + O_{4^oN}}{(13^oN - 4^oN)^2} \tag{15}$$

Once converted from degrees to meters this resulted in $\frac{\partial^2 O}{\partial x^2} = 4.80\times\ 10^{-14}(5.16\times\ 10^{-14})$ ml O_2 l^{-1} m^{-2} and $\frac{\partial^2 O}{\partial y^2} = 5.21\times\ 10^{-13}(4.01\times\ 10^{-13})$ ml O_2 l^{-1} m^{-2} on the 27.1(27.3) isopycnals. K_x and K_y where taken from the original only values of

Table 1 and after converted to days: $K_x = 1.22\times 10^8 (1.12\times 10^8)$ m^2 day^{-1} and $K_y = 6.91\times 10^7 (4.92\times 10^7)$ m^2 day^{-1}.

The vertical gradient was calculated from the WOA13 oxygen data at the test point using the dissolved oxygen concentrations 100 m above and below the climatological depth of each isopycnal: 500(700) m. With depths shown for 27.1 only:

$$\frac{\partial^2 O}{\partial z^2} = \frac{O_{600m} - 2O_{500m} + O_{400m}}{(200m)^2} = 7.50 \times 10^{-6}(-2.00 \times 10^{-5})\frac{mlO_2}{l\ m^2} \tag{16}$$

K_z was taken from Banyte et al. (2012) as 86400 $\times$ 10^{-5} m^2 day^{-1} on both isopycnals.

The biological respiration term was derived from a global dataset of particulate organic carbon (POC) export at the bottom of the euphotic zone calculated by Dunne et al. (2007) with units of $\frac{\mu molO_2}{m^2 day}$. We calculated the vertical decline of this particulate export to the 27.1 and 27.3 isopycnals from the well-known Martin Curve (Martin et al., 1987):

$$\Phi^{POC}(z) = \Phi_0^{POC}(\frac{z}{z_0})^{-b} \tag{17}$$

where $\Phi^{POC}(z)$ is the POC flux at depth z; Φ_0^{POC} the POC flux at the bottom of the euphotic zone (for z_0 = 75m as in Dunne et al. (2007)) and b is the Martin Attenuation Coefficient taken as 0.8 (Bianchi et al., 2012). The depth of each isopycnal was taken from the climatology (WOA13). Assuming that no oxygen is being added by photosynthesis below the euphotic zone and that biological respiration is the only sink of POC between the depths considered, the amount of POC removed from the water column at each isopycnal was calculated as the first derivative of the flux (Equation 17):

$$\frac{d\Phi^{POC}(z)}{dz} = \Phi_0^{POC} z_0^b (-b) z^{-b-1} \tag{18}$$

The amount of carbon remineralized at each isopycnal depth was converted to oxygen consumption rates through the Redfield ratio where O_2:C = 1.3 (Del Giorgio and Duarte, 2002; Cavan et al., 2017; Thomas, 2002). The power law scaling from the Martin curve results in respiration rates that are approximately twice as high on the 27.1 isopycnal as the 27.3.

The resulting values for each term in Equation 13 are displayed in Table 4. THe scale analsyis suggests that the biological consumption term is mostly balanced by meridional diffusion with non-negligible (10-20%) contributions from the vertical and zonal diffusion terms. That the zonal diffusion is small compared to the meridional term despite the larger diffusivity coefficient is not surprising given that the 2nd derivative oxygen gradient is an order of magnitude smaller in the zonal than meridional direction.

Description	**Term**	**27.1** $\left(\frac{mlO_2}{l\ day} \times 10^{-5}\right)$	**27.3** $\left(\frac{mlO_2}{l\ day} \times 10^{-5}\right)$
Biological Consumption	JO	-4.5	-2.2
Zonal Diffusion	$K_x \frac{\partial^2 O}{\partial x^2}$	0.6	0.6
Meridional Diffusion	$K_y \frac{\partial^2 O}{\partial y^2}$	3.6	2.0
Vertical Diffusion	$K_z \frac{\partial^2 O}{\partial z^2}$	0.7	-0.4
Residual		**0.3**	**0.8**

Table 4: Results of the scale analysis at 8.5^{o}N 030^{o}W. Note the negative value in the vertical diffusion on 27.3. Due to the low oxygen core above this isopycnal, vertical diffusivity acts to decrease oxygen on the 27.3 at the test location.

To further probe the importance of these terms to OMZ formation and maintenance, a simple model was constructed to test the hypothesis that the vertical gradient in oxygen between the core of the OMZ and below the core is due to the vertical respiration profile. We used $0.25^o \times 0.25^o$ grid spacing to cover the OMZ area (taken as a box from 4^{o}N - 25^{o}N and 5^{o}W - 45^{o}W) and then shifted

to zonal coordinates of distance from the coast of Africa. The model grid was two-dimensional, except that it utilized climatological (WOA13) data from above and below the study isopycnals to calculate the vertical gradients in oxygen. Two model grids were created to represent the 27.1 and 27.3 isopycnals independent from each other.

The eastern boundary was set to a no zonal flux condition to simulate the west coast of Africa. Zonal and meridional flux was allowed along the northern, western, and southern boundaries that were set to restore oxygen toward the climatological value at an assigned timescale simulating the area outside of the OMZ that is well ventilated due to dynamics not examined here. A 100km (deformation radius) wide region along the eastern boundary was also restored to climatology using the same timescale. In this region, the upwelling and coastal dynamics not examined here serve to restore oxygen, keeping it from reducing to zero. We determined this approach to be reasonable because our study was focused on the mixing in the OMZ away from the coast with no observations in any of these dynamically different boundary regions. For these boundary regions an extra term was added to Equation 12:

$$\frac{dO}{dt} = \frac{1}{\tau}(O_{climatology} - O_{model}) \tag{19}$$

The restoration time scale (τ) served to slowly resupply dissolved oxygen along the boundary of the OMZ to the climatological mean (WOA 2013). For this time scale, we experimented with several different values and found that the best representation of the OMZ was obtained by using 1,000 days. We acknowledge that the vertical term would also require a restoration to climatology as the vertical diffusion would deplete oxygen in the layers above and below. At present, we neglect this detail and simply hold the oxygen levels above and below the subject

isopycnals constant at the climatological value as the vertical supply term provides only about 10% of the total supply. Realistically representing the O_2 depletion and restoration of the oxygen on the adjacent layers would simply decrease this small term further.

Using the same methods as the scale analysis, the respiration rates, lateral gradients, and vertical gradients were calculated for each grid cell in the model space. The vertical oxygen gradients were calculated with the depths in Equation 16 adjusted to the climatological depth of the isopycnal in each grid cell. The respiration rate was held constant throughout time in each grid cell but with the spatial distribution derived from Dunne et al. (2007) and the lateral oxygen gradients were calculated for each model time step based on the previous time step's result. Similar to the scale analysis, we used $K_z = 10^{-5}$ m^2 s^{-1} and K_x and K_y from Table 1 (1410 and 800 m^2 s^{-1}, respectively).

The dissolved oxygen concentration initial condition was set to 3 ml O_2 l^{-1} everywhere and the model concentration reached equilibrium at approximately 30,000 days using a time-step of 5 days to maximize the length of runs and minimize processing time. Figures 17 through 20 show the output of the model using the same diffusivities on each isopycnal ($K_x(K_y) = 1410(800)$ m^2 s^{-1}). Confirming the scale analysis results, the meridional diffusion was the dominant supply term. Figure 19 shows that the model at equilibrium visually matches the shape of the climatology and Figure 20 shows the mean model O_2 concentration to be only 0.15(0.04) ml l^{-1} less than the climatological concentrations on the 27.1(27.3) at equilibrium.

We also explored the sensitivity of the model to several variations. To test the impact of the spatial distribution of biological consumption, we ran the model with the same anisotropic K values on each isopycnal but with a spatially uniform

biological consumption term on each isopycnal (4.5(2.2) $\times 10^{-5}$ ml O_2 l^{-1} day^{-1} on 27.1(27.3)) (i.e. the respiration rate at the central point used to construct the scale analysis in Table 4 was applied to every grid cell). Even with no spatial variability in respiration, the O_2 concentration pattern was virtually identical to the original (not shown). Therefore, only the restoring term, vertical diffusion term, and/or the anisotropic isopycnal diffusivity create this spatial pattern.

To test the sensitivity to the anisotropy in the diffusivity, a run in which the diffusivity was isotropic ($K_x = K_y = 1250$ m^2 s^{-1}) and the same on each isopycnal with the original spatial distribution of biological consumption produced the most accurate results. In this case, the mean model O_2 concentration was found to be 0.03(0.02) ml l^{-1} less(more) than the climatology on the 27.1(27.3) at equilibrium. Due to the imposed isotropy, we increased the meridional diffusivity, which causes higher rates of meridional oxygen transport into the simulated OMZ from the restoring region around the edges. With the restoring region set to climatology, the greater meridional transport leads to a simulated concentration closer to what is seen in nature.

Additionally, to test our hypothesis that the vertical distribution of biological consumption sets the difference in oxygen content between the two isopycnals, the model was run with the 27.3 biological consumption distribution set equal to that on the 27.1. As would be expected from the higher imposed respiration on the 27.3 isopycnal, this change created an average O_2 bias on the 27.3 isopycnal relative to climatology, of 0.27 ml l^{-1} at equilibrium. More importantly, the difference in O_2 concentration on the two isopycnals was only 0.16 ml l^{-1} when respiration was set to be equal, compared to a difference of 0.4 ml l^{-1} when the Martin curve (Equation 18) was used to deduce the respiration rate. The average difference between O_2 concentrations on the two isopycnals in the WOA13 climatology is 0.3

ml l^{-1}, a vertical gradient that can only be simulated when using a respiration rate that declines with depth.

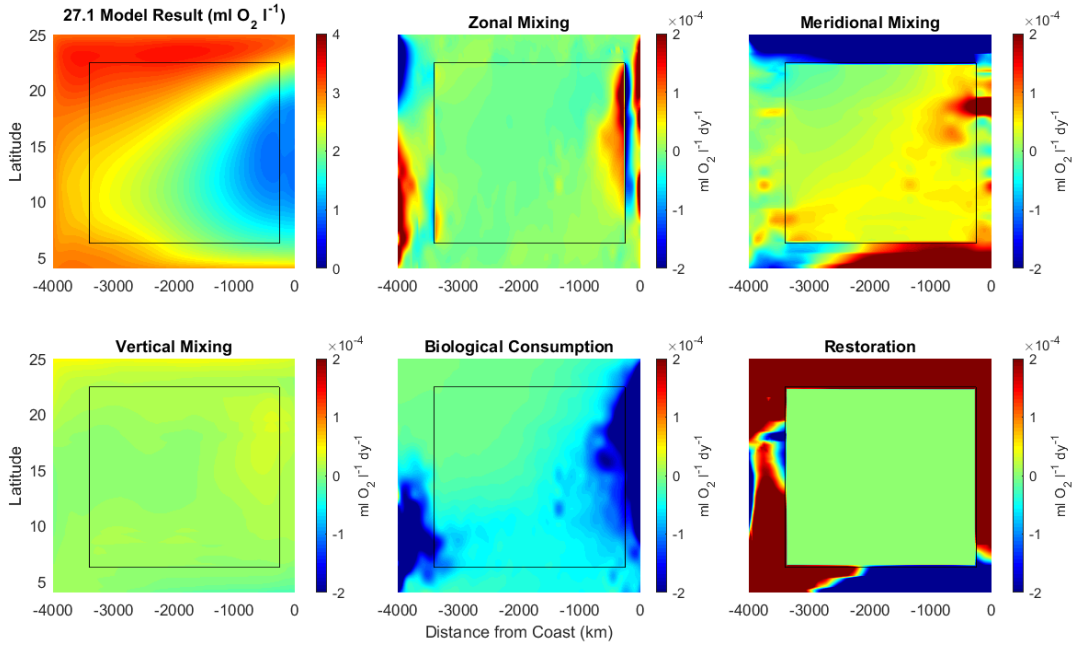

Figure 17: Model output on 27.1 after 40,000 days and 1,000 day restoration timescale. The top left pane shows the oxygen field at equilibrium. The subsequent panes show the spatial contribution of each term at equilibrium. Outside of the black box represents the area in which the restoration term was applied. On each isopycnal, $K_x(K_y) = 1410(800)$ m^2 s^{-1}.

This model exercise demonstrated that by using a parameterized advective time scale on the boundaries of the OMZ to help slowly replenish areas outside of the OMZ where other dynamics exist, we can replicate the shape and intensity of the ETNA OMZ on two isopycnals using only the lateral and vertical mixing terms acting on the large-scale oxygen gradient. In our brief exploration of the various parameters, the model was most impacted by an increased value for meridional diffusivity, supporting the observed result that this is the dominant resupply term. Further,we saw that changing the biological consumption term to match on the two isopycnals made the oxygen concentrations on the two isopycnals much closer

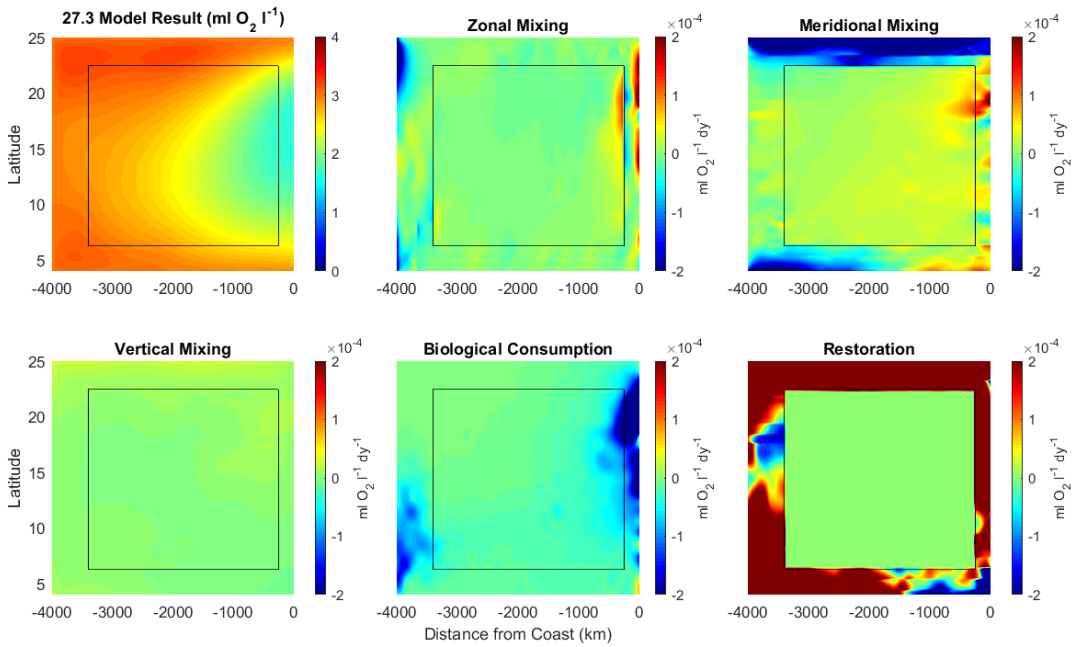

Figure 18: Model output on 27.3 after 40,000 days and 1,000 day restoration timescale. The top left pane shows the oxygen field at equilibrium. The subsequent panes show the spatial contribution of each term at equilibrium. Outside of the black box represents the area in which the restoration term was applied. On each isopycnal, $K_x(K_y) = 1410(800)$ m^2 s^{-1}.

than they are in nature.

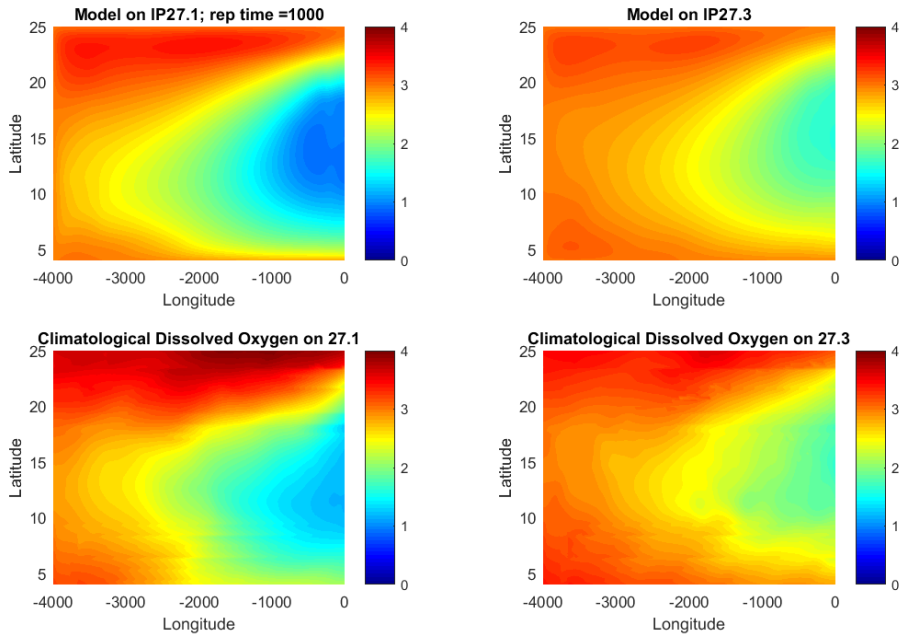

Figure 19: Model output on 27.1 and 27.3 (top) after 40,000 days and 1,000 day restoration timescale compared to the WOA13 dissolved oxygen field interpolated to each isopycnal and shifted to be referenced to distance from the coast.

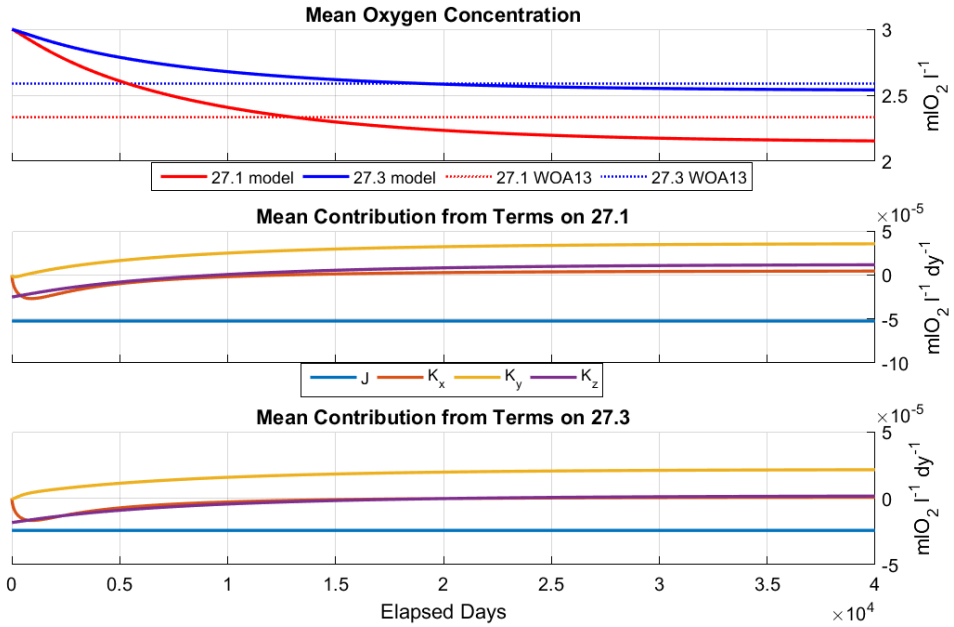

Figure 20: Mean Oxygen concentration (top) on both isopycnals compared to mean climatology and the mean contribution from the supply terms (bottom two panels) through time at equilibrium.

CHAPTER 4

Conclusion

This study used precisely ballasted isopycnal RAFOS floats deployed at the edges of the ETNA OMZ to quantify an isopycnal diffusivity coefficient by two methods. Within the margin of error, the two methods correlated well and showed virtually indistinguishable diffusivity values for the OMZ core isopycnal (σ_θ = 1027.1 kg m^{-3}) and the 1027.3 kg m^{-3} isopycnal below the core. The relative dispersion method showed strong anisotropy with diffusivity in the zonal direction nearly twice as large as in the meridional (1400 m^2 s^{-1} zonally compared to 800 m^2 s^{-1} meridionally). The incorporation of chance pairs provided a diagnostic tool to assess whether a sound source error might have skewed the results, and helped us evaluate the maximum energy containing eddy scale for the system. Despite a higher margin of error, the mean diffusivity value using chance pairs matched well with that resulting from analysis of the original pairs only.

The results from the relative dispersion method were used to probe OMZ formation and maintenance processes in a simple model. The model assumes the advection terms within the OMZ to be negligible and simply restores O_2 concentrations to climatology in a box around the model region where advection is known to play a role in transporting oxygen (upwelling and coastal currents, the subtropical gyre, and the equatorial current bands). Within the OMZ, the sole oxygen supply terms represented are zonal and meridional diffusion, with anisotropic diffusivity values taken from the results of our float analysis, and vertical diffusion, with a diffusivity value taken from a recent intentional tracer release study. This simple representation faithfully simulates the shape and magnitude of O_2 concentrations in the OMZ, as well as the difference in O_2 levels between the two isopycnals. The

model exercise supports the observed result that the dominant supply term for the oxygen budget in the OMZ is meridional mixing, despite a smaller diffusivity in the meridional than zonal direction. Since the diffusivity coefficients were essentially the same at both the oxygen minimum (27.1) isopycnal and beneath it (27.3 isopycnal) within our quantification of error, our model results support that it is the vertical profile of biological oxygen consumption that sets the difference between the two isopycnals. Further work could look at adjusting the boundary conditions and restoration term in the model to probe this assertion in more detail.

Oxygen minimum zones are areas of great biogeochemical importance that could have major impacts on the availability of nitrogen and oceanic sequestration of carbon in a warming climate. Understanding the processes that form and maintain them is crucial to effectively predicting how they may change and what those changes may mean. Our study has provided the first truly Lagrangian study of isopycnal diffusivity in the ETNA OMZ region and found diffusivities that were highly anisotropic and higher than other estimates.

LIST OF REFERENCES

Armi, L., Stommel, H., Armi, L., and Stommel, H. (1983). Four Views of a Portion of the North Atlantic Subtropical Gyre. *Journal of Physical Oceanography*, 13(5):828–857.

Babiano, A., Basdevant, C., and Le Roy A N, P. (1990). Relative dispersion in two-dimensional turbulence. *Journal of Fluid Mechanics*, 214:535–557.

Banyte, D., Tanhua, T., Visbeck, M., Wallace, D. W., Karstensen, J., Krahmann, G., Schneider, A., Stramma, L., and Dengler, M. (2012). Diapycnal diffusivity at the upper boundary of the tropical North Atlantic oxygen minimum zone. *Journal of Geophysical Research: Oceans*, 117(C09016).

Banyte, D., Visbeck, M., Tanhua, T., Fischer, T., Krahmann, G., and Karstensen, J. (2013). Lateral diffusivity from tracer release experiments in the tropical North Atlantic thermocline. *Journal of Geophysical Research: Oceans*, 118:2719–2733.

Batchelor, G. (1952). Diffusion in a field of homogenous turbulence II: The relative motion of particles. *Proceedings of the Cambridge Philosophical Society*, 48:345–362.

Bianchi, D., Dunne, J. P., Sarmiento, J. L., and Galbraith, E. D. (2012). Data-based estimates of suboxia, denitrification, and N2O production in the ocean and their sensitivities to dissolved O2. *Global Biogeochemical Cycles*, 26(2).

Brandt, P., Bange, H. W., Banyte, D., Dengler, M., Didwischus, S. H., Fischer, T., Greatbatch, R. J., Hahn, J., Kanzow, T., Karstensen, J., Körtzinger, A., Krahmann, G., Schmidtko, S., Stramma, L., Tanhua, T., and Visbeck, M. (2015). On the role of circulation and mixing in the ventilation of oxygen minimum zones with a focus on the eastern tropical North Atlantic. *Biogeosciences*, 12:489–512.

Brandt, P., Greatbatch, R. J., Claus, M., Didwischus, S. H., Hormann, V., Funk, A., Hahn, J., Krahmann, G., Fischer, J., and Krtzinger, A. (2012). Ventilation of the equatorial Atlantic by the equatorial deep jets. *Journal of Geophysical Research: Oceans*, 117(C12015).

Brandt, P., Hormann, V., Körtzinger, A., Visbeck, M., Krahmann, G., Stramma, L., Lumpkin, R., and Schmid, C. (2010). Changes in the Ventilation of the Oxygen Minimum Zone of the Tropical North Atlantic. *Journal of Physical Oceanography*, 40:1784–1801.

Cavan, E. L., Trimmer, M., Shelley, F., and Sanders, R. (2017). Remineralization of particulate organic carbon in an ocean oxygen minimum zone. *Nature Communications*, 8(14847).

Codispoti, L. A., Brandes, J., P. Christensen, J., Devol, A., Naqvi, S. W. A., Paerl, H., and Yoshinari, T. (2001). The Oceanic Fixed Nitrogen and Nitrous Oxide Budgets: Moving Targets as We Enter the Anthropocene? *Scientia Marina*, 65:85–105.

Cole, S. T., Wortham, C., Kunze, E., and Owens, W. B. (2015). Eddy stirring and horizontal diffusivity from Argo float observations: Geographic and depth variability. *Geophysical Research Letters*, 42:3989–3997.

Cushman-Roisin, B. and Beckers, J.-M. (2011). *Introduction to geophysical fluid dynamics : physical and numerical aspects*. Academic Press.

Del Giorgio, P. A. and Duarte, C. M. (2002). Respiration in the open ocean. *Nature*, 420:379–384.

Deutsch, C., Brix, H., Ito, T., Frenzel, H., and Thompson, L. (2011). Climate-Forced Variability of Ocean Hypoxia. *Science*, 333(6040):336–339.

Deutsch, C., Ferrel, A., Seibel, B., Portner, H.-O., and Huey, R. B. (2015). Climate change tightens a metabolic constraint on marine habitats. *Science*, 348(6239):1132–1135.

Ferrari, R. and Polzin, K. L. (2005). Finescale Structure of the TS Relation in the Eastern North Atlantic. *Journal of Physical Oceanography*, 35:1437–1454.

Fischer, T., Banyte, D., Brandt, P., Dengler, M., Krahmann, G., Tanhua, T., and Visbeck, M. (2013). Diapycnal oxygen supply to the tropical North Atlantic oxygen minimum zone. *Biogeosciences*, 10:5079–5093.

Garcia, H. E., Locarnini, R. A., Boyer, T. P., Antonov, J. I., Mishonov, A. V., Baranova, O. K., Zweng, M. M., Reagan, J. R., Johnson, D. R., Levitus, S. E., and Mishonov, A. T. E. (2013). World Ocean Atlas 2013. Vol. 3: Dissolved Oxygen, Apparent Oxygen Utilization, and Oxygen Saturation. *NOAA Atlas NESDIS*, 75:27 pp.

Garrett, C. (1983). On the initial streakiness of a dispersion tracer in two- and three-dimensional turbulence. *Dynamics of Atmosphere and Oceans*, 7:265–277.

Gnanadesikan, A., Bianchi, D., and Pradal, M. A. (2013). Critical role for mesoscale eddy diffusion in supplying oxygen to hypoxic ocean waters. *Geophysical Research Letters*, 40:5194–5198.

Hahn, J., Brandt, P., Greatbatch, R. J., Krahmann, G., and Körtzinger, A. (2014). Oxygen variance and meridional oxygen supply in the Tropical North East Atlantic oxygen minimum zone. *Climate Dynamics*, 43:2999–3024.

Klocker, A., Ferrari, R., Lacasce, J. H., and Merrifield, S. T. (2012). Reconciling float-based and tracer-based estimates of lateral diffusivities. *Journal of Marine Research*, 70:569–602.

Kolmogorov, A. (1941). The local structure of turbulence in incompressible visouc fluid for very large reynolds numbers,. *Doklady Akademii Nauk SSSR*, 30:299–303.

LaCasce, J. H. (2008). Statistics from Lagrangian observations. *Progress in Oceanography*, 77:1–29.

LaCasce, J. H. and Bower, A. (2000). Relative dispersion in the subsurface North Atlantic. *Journal of Marine Research*, 58:863–894.

Ledwell, J. R., Watson, A. J., and Law, C. S. (1998). Mixing of a tracer in the pycnocline. *Journal of Geophysical Research: Oceans*, 103(C10):21499–21529.

Locarnini, R. A., Mishonov, A. V., Antonov, J. I., Boyer, T. P., Garcia, H. E., Baranova, O. K., Zweng, M. M., Paver, C. R., Reagan, J. R., Johnson, D. R., Hamilton, M., Seidov, D., Levitus, S, E., and Mishonov, A., T. E. (2013). World Ocean Atlas 2013, Volume 1: Temperature. *NOAA Atlas NESDIS*, 73:44pp.

Lumpkin, R. and Elipot, S. (2010). Surface drifter pair spreading in the North Atlantic. *Journal of Geophysical Research: Oceans*, 115(C12017).

Luyten, J. R., Pedlosky, J., Stommel, H., Luyten, J. R., Pedlosky, J., and Stommel, H. (1983). The Ventilated Thermocline. *Journal of Physical Oceanography*, 13(2):292–309.

Martin, J. H., Knauer, G. A., Karl, D. M., and Broenkow, W. W. (1987). VERTEX: carbon cycling in the northeast Pacific. *Deep Sea Research Part A. Oceanographic Research Papers*, 34(2):267–285.

Maximenko, N. A., Melnichenko, O. V., Niiler, P. P., and Sasaki, H. (2008). Stationary mesoscale jet-like features in the ocean. *Geophysical Research Letters*, 35(L08603,).

Nakamura, N. (2008). Quantifying Inhomogeneous, Instantaneous, Irreversible Transport Using Passive Tracer Field as a Coordinate. In *Transport and Mixing in Geophysical Flows*, pages 137–164. Springer Berlin Heidelberg, Berlin, Heidelberg.

Ollitrault, M., Lankhorst, M., Fratantoni, D., Richardson, P., and Zenk, W. (2006). Zonal intermediate currents in the equatorial Atlantic Ocean. *Geophysical Research Letters*, 33(L05605).

Peña-Izquierdo, J., Van Sebille, E., Pelegrí, J. L., Sprintall, J., Mason, E., Llanillo, P. J., and Machín, F. (2015). Water mass pathways to the North Atlantic oxygen minimum zone. *Journal of Geophysical Research: Oceans*, 120:3350–3372.

Richardson, L. (1926). Atmospheric diffusion on a distance-neighbour graph. *Proceedings of the Royal Society of London Series A*, 110:709–737.

Rossby, T., Dorson, D., and Fontaine, J. (1986). The RAFOS System. *Journal of Atmospheric and Oceanic Technology*, 3:672–679.

Rypina, I. I., Kamenkovich, I., Berloff, P., and Pratt, L. J. (2012). Eddy-Induced Particle Dispersion in the Near-Surface North Atlantic. *Journal of Physical Oceanography*, 42:2206–2228.

Siedler, G., Zangenberg, N., Onken, R., and Morlière, A. (1992). Seasonal changes in the tropical Atlantic circulation: Observation and simulation of the Guinea Dome. *Journal of Geophysical Research*, 97(C1):703–715.

Stramma, L., Czeschel, R., Tanhua, T., Brandt, P., Visbeck, M., and Giese, B. S. (2016). The flow field of the upper hypoxic eastern tropical North Atlantic oxygen minimum zone. *Ocean Science*, 12:153–167.

Taylor, G. (1921). Diffusion by continuous movements. *Procedings of the London Mathematics Society, Series A*, 20:196–221.

Thomas, H. (2002). Remineralization ratios of carbon, nutrients, and oxygen in the North Atlantic Ocean: A field databased assessment. *Global Biogeochemical Cycles*, 16(3).

Thomas, H., Bozec, Y., Elkalay, K., and Hein J W de Baar. (2004). Enhanced Open Ocean Storage of CO2 from Shelf Sea Pumping. *Science*, 304(5673):1005–1008.

Wunsch, C. (1999). Where do ocean eddy heat fluxes matter? *Journal of Geophysical Research: Oceans*, 104(C6):13235–13249.

APPENDIX

Supplemental Figures

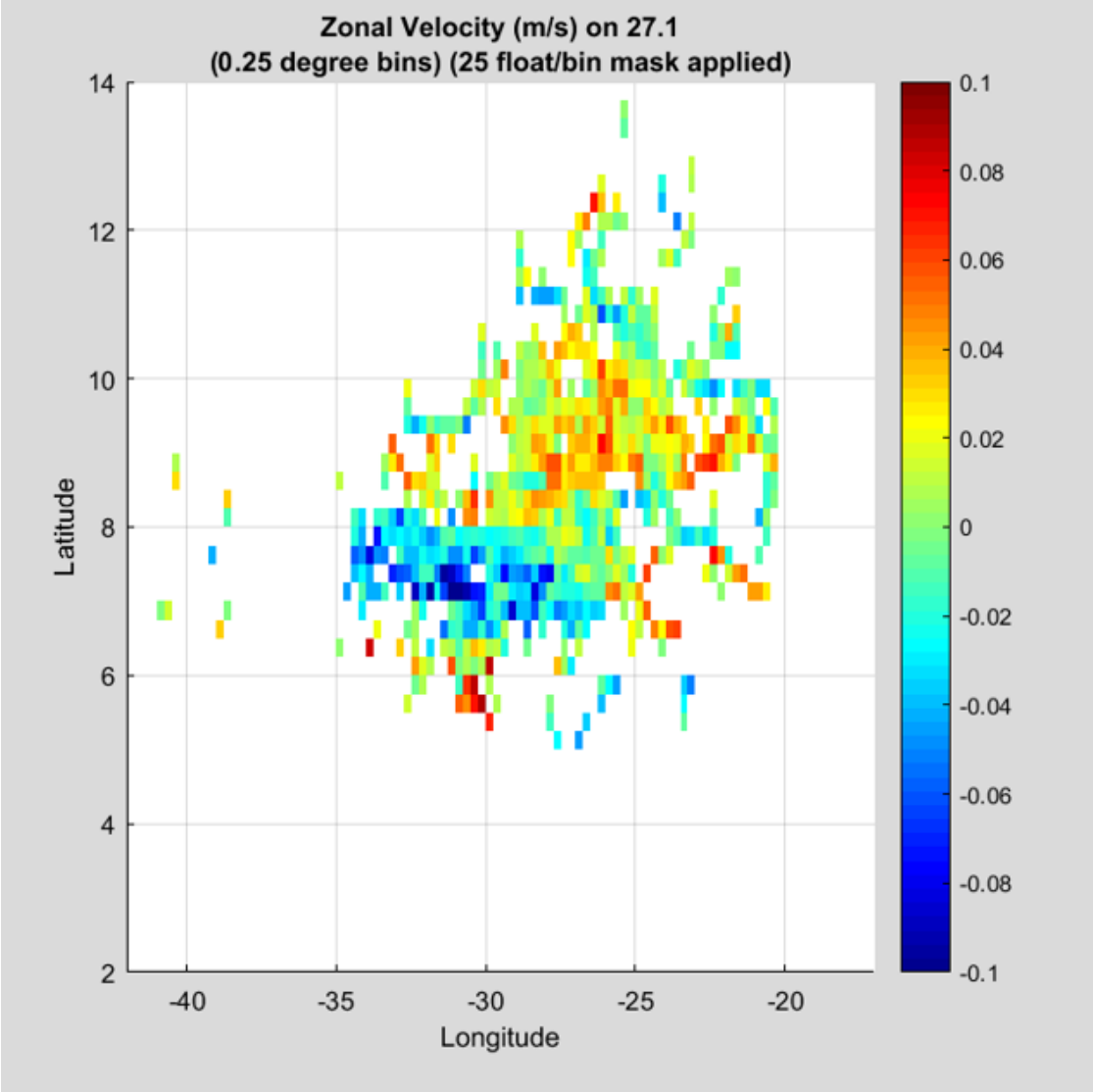

Figure A.1: Mean zonal velocity field (m s^{-1}) on the 27.1 isopycnal calculated from float positions in 0.25^o with a 25 float record per bin threshold applied. Note the zonal signature of an anti-cyclonic circulation.

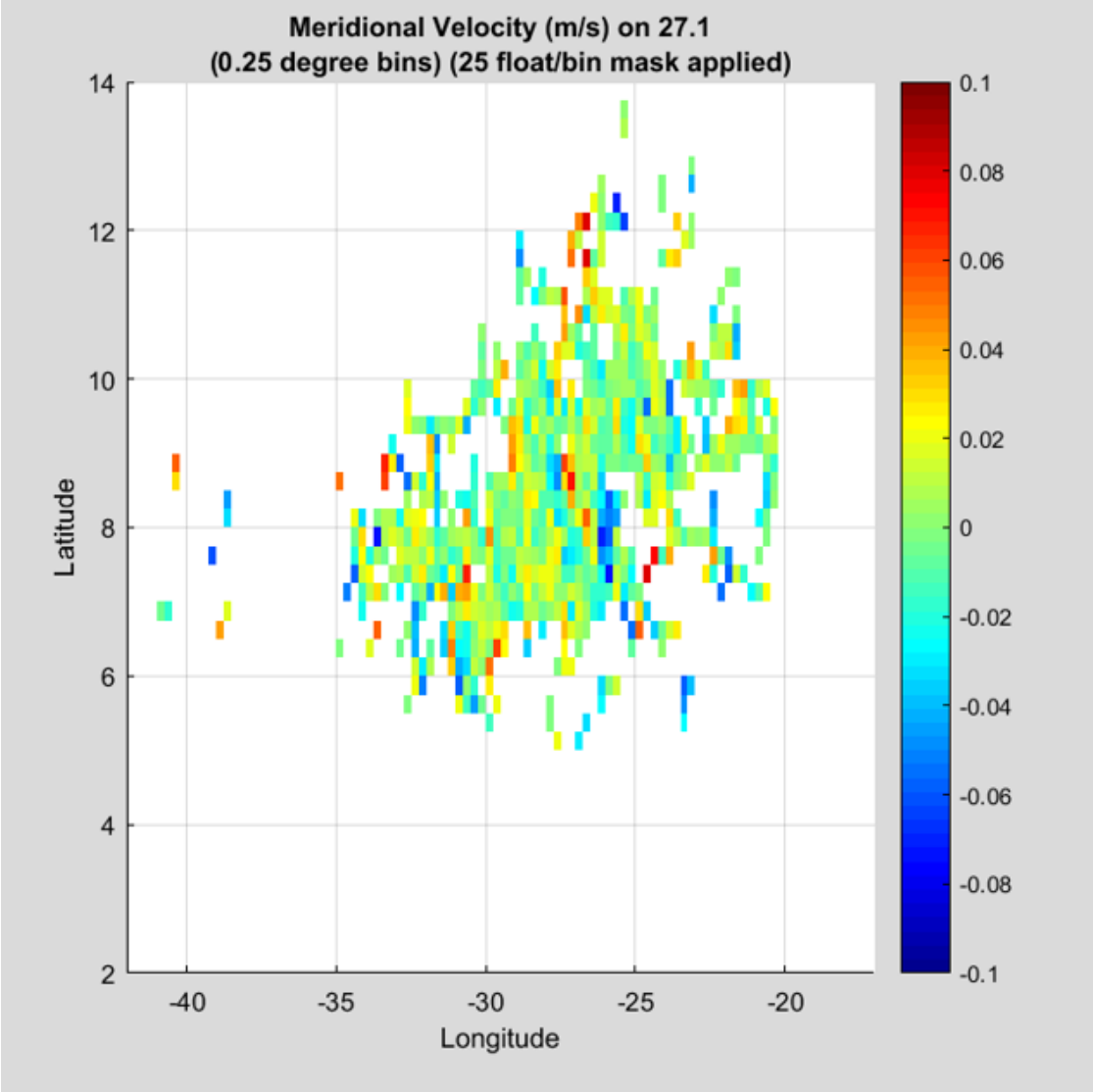

Figure A.2: Mean meridional velocity field (m s^{-1}) on the 27.1 isopycnal calculated from float positions in 0.25^o with a 25 float record per bin threshold applied.

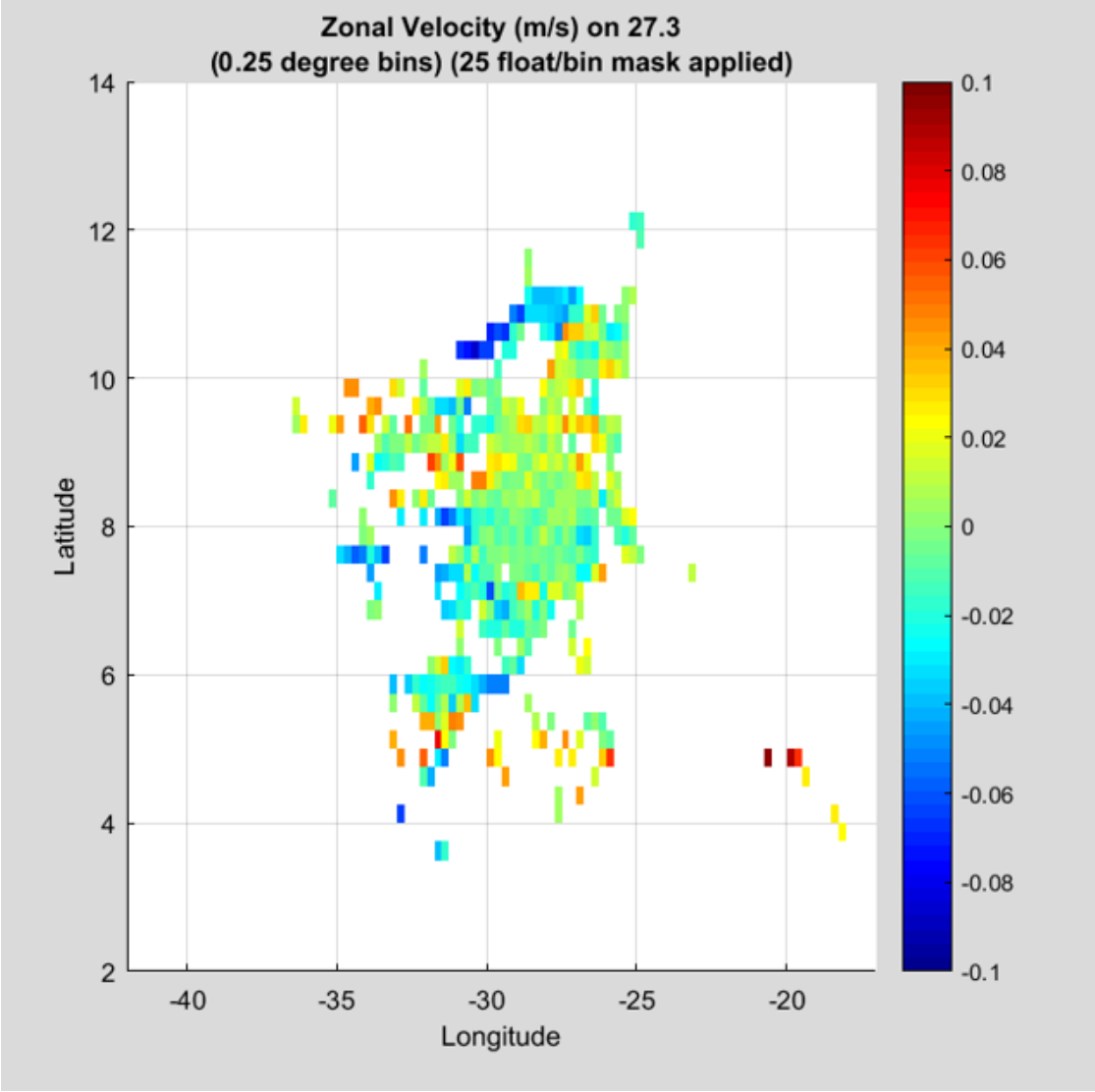

Figure A.3: Mean zonal velocity field (m s^{-1}) on the 27.3 isopycnal calculated from float positions in 0.25^o with a 25 float record per bin threshold applied.

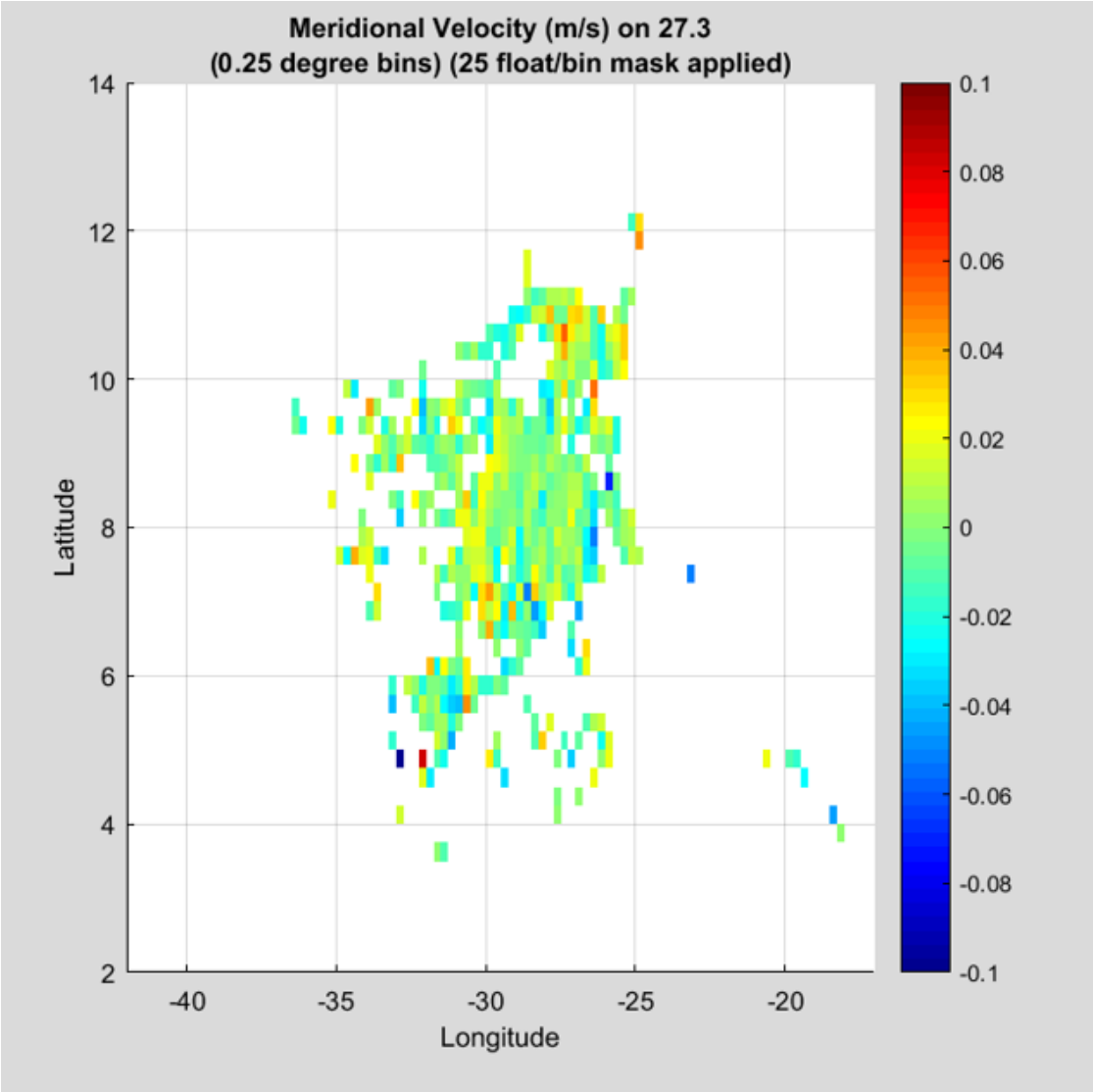

Figure A.4: Mean meridional velocity field (m s^{-1}) on the 27.3 isopycnal calculated from float positions in 0.25^o with a 25 float record per bin threshold applied.

	Pairs	Effective Diffusivity (m^2 s^{-1}) K	Kx	Ky
Original Only				
27.1	145	**1254**	**1410**	**800**
		± 518	± 493	± 313
Length Scale (km)		90	80	40
27.3	119	**1484**	**1297**	**570**
		± 980	± 630	±364
Length Scale (km)		100	75	40
Chance Only	**10km**	**5 days**	10 day start	
27.1	115	**1198**	**1418**	**357**
		± 1154	± 1000	± 563
Length Scale (km)		100	80	50
27.3	92	**1417**	**1305**	**300**
		± 1271	± 1277	±250
Length Scale (km)		100	80	40
Chance + Orig	**10km**	**5 days**		
27.1	296	**1654**	**1747**	**541**
		±624	± 619	± 376
Length Scale (km)		100	100	70
27.3	211	**1652**	**1479**	**646**
		±768	±855	±884
Length scale (km)		100	100	70
Chance Only	**10km**	**3 days**	10 day start	
27.1	161	**1161**	**1463**	**481**
		± 909	± 968	± 528
Length Scale (km)		100	100	55
27.3	123	**1393**	**1365**	**154**
		± 1022	± 888	±905
Length scale		100	90	35
Chance Only	**10km**	**10 days**	10 day start	
27.1	69	**1067**	**1256**	**97**
		± 1571	± 1401	± 850
Length Scale (km)		100	97	70
27.3	68	**1214**	**1272**	**526**
		± 1632	± 1428	± 488
Length Scale (km)		96	98	52
Chance Only	**25km**	**5 days**	10 day start	
27.1	147	**2004**	**2076**	**723**
		±1097	±1319	± 459
Length Scale (km)		116	107	50
27.3	157	**1328**	**1477**	**648**
		± 1414	± 1278	± 478
Length Scale (km)		140	99	55
Chance Only	**5km**	**5 days**	10 day start	
27.1	99	**1094**	**1058**	**645**
		± 1111	± 1170	± 1520
Length Scale (km)		101	98	53
27.3	68	**1158**	**1013**	**337**
		±1783	± 1159	± 843
Length Scale (km)		101	87	61

Table A.1: Results of the diffusivity calculations from relative dispersion in m^2 s^{-1}. The number of pairings on each isopycnal using each set of parameters is listed in the second column. The "chance pair only" calculations considered only new pairs starting after the 10th mission day to exclude original pairs. The thresholds used to identify chance pairings are identified in the heading rows. The ± rows are from the 90% confidence limit. The length scale rows identify the decorrelation length scale (km) used for each estimation.

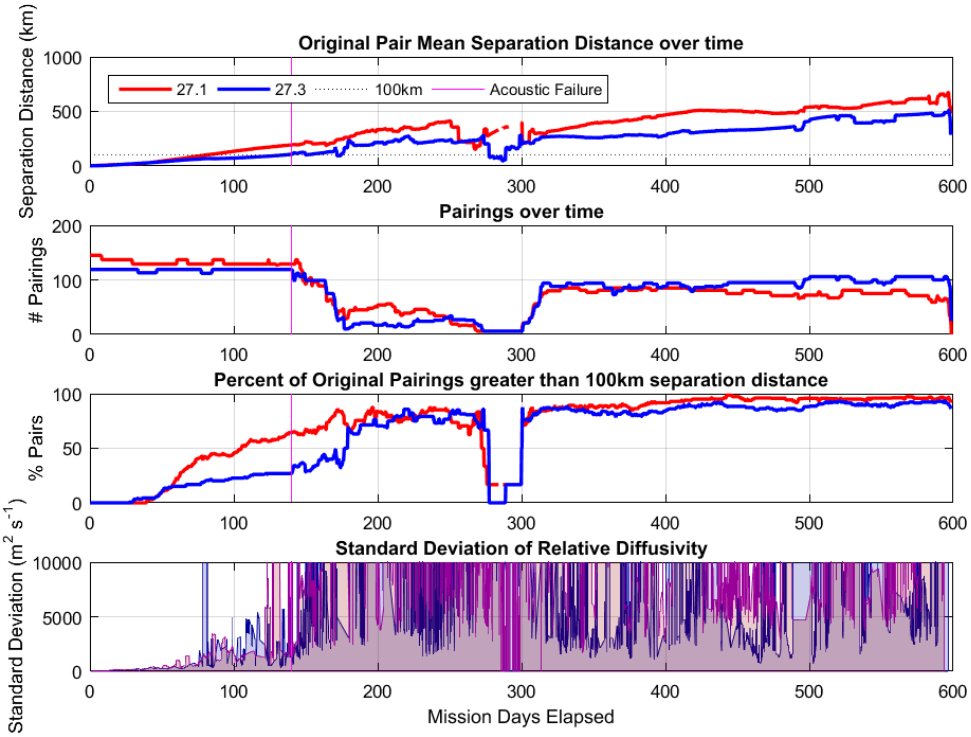

Figure A.5: Float Pairing diagnostics for original pairs only.

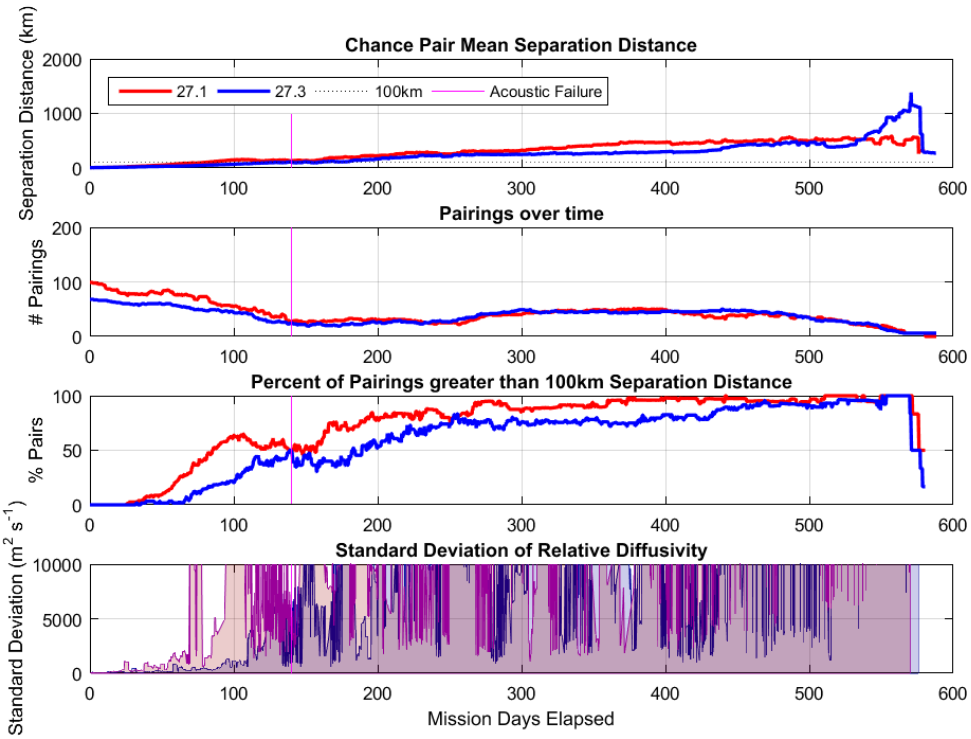

Figure A.6: Float Pairing diagnostics for chance pairs only. The chance pairings here were identified using a 10km and 5day threshold.

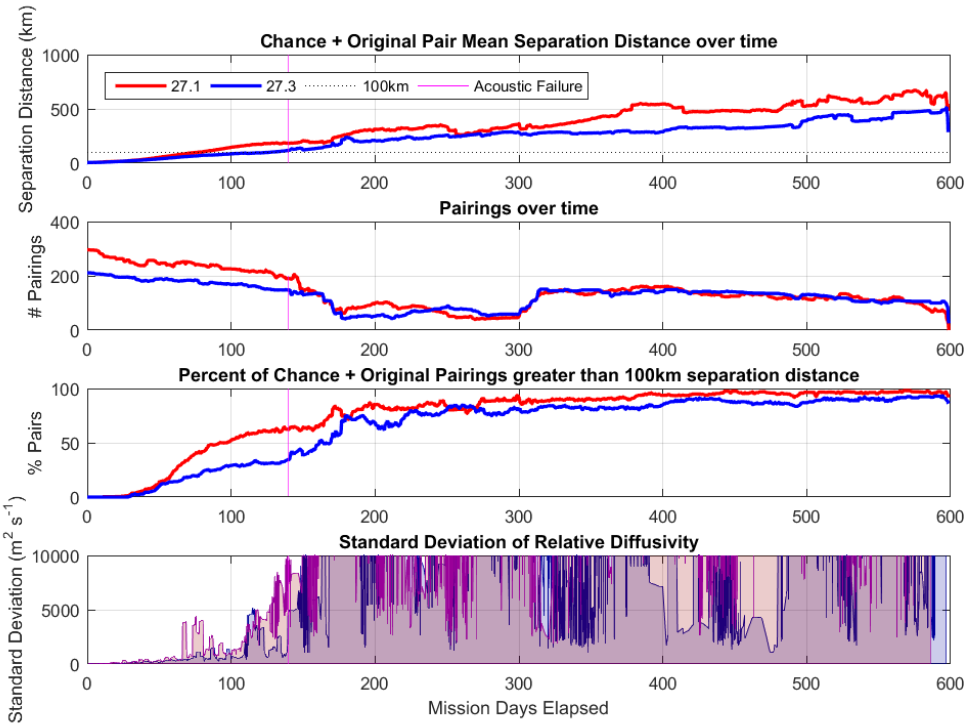

Figure A.7: Float Pairing diagnostics for a combination of chance and original pairs. The chance pairings here were identified using a 10km and 5day threshold.

BIBLIOGRAPHY

Armi, L., Stommel, H., Armi, L., and Stommel, H., "Four Views of a Portion of the North Atlantic Subtropical Gyre," *Journal of Physical Oceanography*, vol. 13, no. 5, pp. 828–857, 5 1983. [Online]. Available: http://journals.ametsoc.org/doi/abs/10.1175/1520-0485%281983%29013%3C0828%3AFVOAPO%3E2.0.CO%3B2

Babiano, A., Basdevant, C., and Le Roy A N, P., "Relative dispersion in two-dimensional turbulence," *Journal of Fluid Mechanics*, vol. 214, pp. 535–557, 1990. [Online]. Available: https://www.cambridge.org/core/services/aop-cambridge-core/content/view/A96F4F8C7B65DFDC85B0E00B039C536B/S0022112090000258a.pdf/relative_dispersion_in_twodimensional_turbulence.pdf

Banyte, D., Tanhua, T., Visbeck, M., Wallace, D. W., Karstensen, J., Krahmann, G., Schneider, A., Stramma, L., and Dengler, M., "Diapycnal diffusivity at the upper boundary of the tropical North Atlantic oxygen minimum zone," *Journal of Geophysical Research: Oceans*, vol. 117, no. C09016, 2012.

Banyte, D., Visbeck, M., Tanhua, T., Fischer, T., Krahmann, G., and Karstensen, J., "Lateral diffusivity from tracer release experiments in the tropical North Atlantic thermocline," *Journal of Geophysical Research: Oceans*, vol. 118, pp. 2719–2733, 2013.

Batchelor, G., "Diffusion in a field of homogenous turbulence II: The relative motion of particles," *Proceedings of the Cambridge Philosophical Society*, vol. 48, pp. 345–362, 1952.

Bianchi, D., Dunne, J. P., Sarmiento, J. L., and Galbraith, E. D., "Data-based estimates of suboxia, denitrification, and N2O production in the ocean and their sensitivities to dissolved O2," *Global Biogeochemical Cycles*, vol. 26, no. 2, 2012.

Brandt, P., Bange, H. W., Banyte, D., Dengler, M., Didwischus, S. H., Fischer, T., Greatbatch, R. J., Hahn, J., Kanzow, T., Karstensen, J., Körtzinger, A., Krahmann, G., Schmidtko, S., Stramma, L., Tanhua, T., and Visbeck, M., "On the role of circulation and mixing in the ventilation of oxygen minimum zones with a focus on the eastern tropical North Atlantic," *Biogeosciences*, vol. 12, pp. 489–512, 2015.

Brandt, P., Greatbatch, R. J., Claus, M., Didwischus, S. H., Hormann, V., Funk, A., Hahn, J., Krahmann, G., Fischer, J., and Krtzinger, A., "Ventilation of the equatorial Atlantic by the equatorial deep jets," *Journal of Geophysical Research: Oceans*, vol. 117, no. C12015, 2012.

Brandt, P., Hormann, V., Körtzinger, A., Visbeck, M., Krahmann, G., Stramma, L., Lumpkin, R., and Schmid, C., "Changes in the Ventilation of the Oxygen Minimum Zone of the Tropical North Atlantic," *Journal of Physical Oceanography*, vol. 40, pp. 1784–1801, 2010.

Cavan, E. L., Trimmer, M., Shelley, F., and Sanders, R., "Remineralization of particulate organic carbon in an ocean oxygen minimum zone," *Nature Communications*, vol. 8, no. 14847, 2017.

Chelton, D. B., deSzoeke, R. A., Schlax, M. G., El Naggar, K., Siwertz, N., Chelton, D. B., deSzoeke, R. A., Schlax, M. G., Naggar, K. E., and Siwertz, N., "Geographical Variability of the First Baroclinic Rossby Radius of Deformation," *Journal of Physical Oceanography*, vol. 28, no. 3, pp. 433–460, 3 1998. [Online]. Available: http://journals.ametsoc.org/doi/abs/10.1175/1520-0485%281998%29028%3C0433%3AGVOTFB%3E2.0.CO%3B2

Codispoti, L. A., Brandes, J., P. Christensen, J., Devol, A., Naqvi, S. W. A., Paerl, H., and Yoshinari, T., "The Oceanic Fixed Nitrogen and Nitrous Oxide Budgets: Moving Targets as We Enter the Anthropocene?" *Scientia Marina*, vol. 65, pp. 85–105, 4 2001.

Cole, S. T., Wortham, C., Kunze, E., and Owens, W. B., "Eddy stirring and horizontal diffusivity from Argo float observations: Geographic and depth variability," *Geophysical Research Letters*, vol. 42, pp. 3989–3997, 2015.

Cushman-Roisin, B. and Beckers, J.-M., *Introduction to geophysical fluid dynamics : physical and numerical aspects*. Academic Press, 2011.

D'asaro, E. A. and Mcneil, C., "Calibration and Stability of Oxygen Sensors on Autonomous Floats 1," 2013. [Online]. Available: https://www.aanderaa.com/media/pdfs/asaro-and-mc-niel-2013-calibration-and-stability-of-o2-sensors-on-floats-submitted.pdf

Del Giorgio, P. A. and Duarte, C. M., "Respiration in the open ocean," *Nature*, vol. 420, pp. 379–384, 2002.

Deutsch, C., Ferrel, A., Seibel, B., Portner, H.-O., and Huey, R. B., "Climate change tightens a metabolic constraint on marine habitats," *Science*, vol. 348, no. 6239, pp. 1132–1135, 6 2015. [Online]. Available: http://www.sciencemag.org/cgi/doi/10.1126/science.aaa1605

Deutsch, C., Brix, H., Ito, T., Frenzel, H., and Thompson, L., "Climate-Forced Variability of Ocean Hypoxia," *Science*, vol. 333, no. 6040, pp. 336–339, 2011. [Online]. Available: http://science.sciencemag.org.uri.idm.oclc.org/content/sci/333/6040/336.full.pdf

Dunne, J. P., Sarmiento, J. L., and Gnanadesikan, A., "A synthesis of global particle export from the surface ocean and cycling through the ocean interior and on the seafloor," *Global Biogeochemical Cycles*, 2007.

Ferrari, R. and Polzin, K. L., "Finescale Structure of the TS Relation in the Eastern North Atlantic," *Journal of Physical Oceanography*, vol. 35, pp. 1437–1454, 2005.

Fischer, T., Banyte, D., Brandt, P., Dengler, M., Krahmann, G., Tanhua, T., and Visbeck, M., "Diapycnal oxygen supply to the tropical North Atlantic oxygen minimum zone," *Biogeosciences*, vol. 10, pp. 5079–5093, 2013.

Garcia, H. E., Locarnini, R. A., Boyer, T. P., Antonov, J. I., Mishonov, A. V., Baranova, O. K., Zweng, M. M., Reagan, J. R., Johnson, D. R., Levitus, S. E., and Mishonov, A. T. E., "World Ocean Atlas 2013. Vol. 3: Dissolved Oxygen, Apparent Oxygen Utilization, and Oxygen Saturation," *NOAA Atlas NESDIS*, vol. 75, p. 27 pp, 2013. [Online]. Available: https://data.nodc.noaa.gov/woa/WOA13/DOC/woa13_vol3.pdf

Garrett, C., "On the initial streakiness of a dispersion tracer in two- and three-dimensional turbulence," *Dynamics of Atmosphere and Oceans*, vol. 7, pp. 265–277, 1983.

Gnanadesikan, A., Bianchi, D., and Pradal, M. A., "Critical role for mesoscale eddy diffusion in supplying oxygen to hypoxic ocean waters," *Geophysical Research Letters*, vol. 40, pp. 5194–5198, 2013.

Hahn, J., Brandt, P., Greatbatch, R. J., Krahmann, G., and Körtzinger, A., "Oxygen variance and meridional oxygen supply in the Tropical North East Atlantic oxygen minimum zone," *Climate Dynamics*, vol. 43, pp. 2999–3024, 2014.

Klocker, A., Ferrari, R., Lacasce, J. H., and Merrifield, S. T., "Reconciling float-based and tracer-based estimates of lateral diffusivities," *Journal of Marine Research*, vol. 70, pp. 569–602, 2012.

Kolmogorov, A., "The local structure of turbulence in incompressible visouc fluid for very large reynolds numbers,," *Doklady Akademii Nauk SSSR*, vol. 30, pp. 299–303, 1941.

LaCasce, J. H., "Statistics from Lagrangian observations," *Progress in Oceanography*, vol. 77, pp. 1–29, 2008.

LaCasce, J. H. and Bower, A., "Relative dispersion in the subsurface North Atlantic," *Journal of Marine Research*, vol. 58, pp. 863–894, 2000.

Ledwell, J. R., Watson, A. J., and Law, C. S., "Mixing of a tracer in the pycnocline," *Journal of Geophysical Research: Oceans*, vol. 103, no. C10, pp. 21 499–21 529, 1998.

Locarnini, R. A., Mishonov, A. V., Antonov, J. I., Boyer, T. P., Garcia, H. E., Baranova, O. K., Zweng, M. M., Paver, C. R., Reagan, J. R., Johnson, D. R., Hamilton, M., Seidov, D., Levitus, S, E., and Mishonov, A., T. E., "World Ocean Atlas 2013, Volume 1: Temperature," *NOAA Atlas NESDIS*, vol. 73, p. 44pp, 2013. [Online]. Available: https://data.nodc.noaa.gov/woa/WOA13/DOC/woa13_vol1.pdf

Lumpkin, R. and Elipot, S., "Surface drifter pair spreading in the North Atlantic," *Journal of Geophysical Research: Oceans*, vol. 115, no. C12017, 2010.

Luyten, J. R., Pedlosky, J., Stommel, H., Luyten, J. R., Pedlosky, J., and Stommel, H., "The Ventilated Thermocline," *Journal of Physical Oceanography*, vol. 13, no. 2, pp. 292–309, 2 1983. [Online]. Available: http://journals.ametsoc.org/doi/abs/10.1175/1520-0485%281983%29013%3C0292%3ATVT%3E2.0.CO%3B2

Martin, J. H., Knauer, G. A., Karl, D. M., and Broenkow, W. W., "VERTEX: carbon cycling in the northeast Pacific," *Deep Sea Research Part A. Oceanographic Research Papers*, vol. 34, no. 2, pp. 267–285, 2 1987. [Online]. Available: https://www.sciencedirect.com/science/article/pii/0198014987900860

Maximenko, N. A., Melnichenko, O. V., Niiler, P. P., and Sasaki, H., "Stationary mesoscale jet-like features in the ocean," *Geophysical Research Letters*, vol. 35, no. L08603,, 2008.

Nakamura, N., "Quantifying Inhomogeneous, Instantaneous, Irreversible Transport Using Passive Tracer Field as a Coordinate," in *Transport and Mixing in Geophysical Flows*. Berlin, Heidelberg: Springer Berlin Heidelberg, 2008, pp. 137–164. [Online]. Available: http://link.springer.com/10.1007/978-3-540-75215-8_7

Ollitrault, M., Lankhorst, M., Fratantoni, D., Richardson, P., and Zenk, W., "Zonal intermediate currents in the equatorial Atlantic Ocean," *Geophysical Research Letters*, vol. 33, no. L05605, 2006.

Peña-Izquierdo, J., Van Sebille, E., Pelegrí, J. L., Sprintall, J., Mason, E., Llanillo, P. J., and Machín, F., "Water mass pathways to the North Atlantic oxygen minimum zone," *Journal of Geophysical Research: Oceans*, vol. 120, pp. 3350–3372, 2015.

Richardson, L., "Atmospheric diffusion on a distance-neighbour graph," *Proceedings of the Royal Society of London Series A*, vol. 110, pp. 709–737, 1926.

Rossby, T., Dorson, D., and Fontaine, J., "The RAFOS System," *Journal of Atmospheric and Oceanic Technology*, vol. 3, pp. 672–679, 1986.

Rypina, I. I., Kamenkovich, I., Berloff, P., and Pratt, L. J., "Eddy-Induced Particle Dispersion in the Near-Surface North Atlantic," *Journal of Physical Oceanography*, vol. 42, pp. 2206–2228, 2012. [Online]. Available: https://journals.ametsoc.org/doi/pdf/10.1175/JPO-D-11-0191.1

Siedler, G., Zangenberg, N., Onken, R., and Morlière, A., "Seasonal changes in the tropical Atlantic circulation: Observation and simulation of the Guinea Dome," *Journal of Geophysical Research*, vol. 97, no. C1, pp. 703–715, 1992.

Stramma, L., Czeschel, R., Tanhua, T., Brandt, P., Visbeck, M., and Giese, B. S., "The flow field of the upper hypoxic eastern tropical North Atlantic oxygen minimum zone," *Ocean Science*, vol. 12, pp. 153–167, 2016.

Stramma, L., Johnson, G. C., Sprintall, J., and Mohrholz, V., "Expanding oxygen-minimum zones in the tropical oceans," *Science*, 2008.

Taylor, G., "Diffusion by continuous movements," *Procedings of the London Mathematics Society, Series A*, vol. 20, pp. 196–221, 1921.

Thomas, H., "Remineralization ratios of carbon, nutrients, and oxygen in the North Atlantic Ocean: A field databased assessment." *Global Biogeochemical Cycles*, vol. 16, no. 3, 2002.

Thomas, H., Bozec, Y., Elkalay, K., and Hein J W de Baar., "Enhanced Open Ocean Storage of CO2 from Shelf Sea Pumping," *Science*, vol. 304, no. 5673, pp. 1005–1008, 2004. [Online]. Available: https://search-proquest-com.uri.idm.oclc.org/docview/213578437/fulltextPDF/C09F96484DF04F6CPQ/75?accountid=28991

Wunsch, C., "Where do ocean eddy heat fluxes matter?" *Journal of Geophysical Research: Oceans*, vol. 104, no. C6, pp. 13 235–13 249, 1999.